Journal of Experimental Botany
doi:10.1093/jxb/erx033

RESEARCH PAPER

RING-H2-type E3 gene *VpRH2* from *Vitis pseudoreticulata* improves resistance to powdery mildew by interacting with VpGRP2A

Lei Wang[1,2,3,†], Xiaoqing Xie[1,2,3,†], Wenkong Yao[1,2,3,†], Jie Wang[1,2,3], Fuli Ma[1,2,3], Chen Wang[1,2,3], Yazhou Yang[1,2,3], Weihuo Tong[1,2,3], Jianxia Zhang[1,2,3], Yan Xu[1,2,3], Xiping Wang[1,2,3], Chaohong Zhang[1,2,3,*] and Yuejin Wang[1,2,3,*]

[1] College of Horticulture, Northwest A & F University, Yangling, Shaanxi, 712100, the People's Republic of China
[2] Key Laboratory of Horticultural Plant Biology and Germplasm Innovation in Northwest China, Ministry of Agriculture, Yangling, Shaanxi 712100, the People's Republic of China
[3] State Key Laboratory of Crop Stress Biology in Arid Areas, Northwest A & F University, Yangling, Shaanxi, 712100, the People's Republic of China

* Correspondence: zhangchaohong@nwsuaf.edu.cn and wangyj@nwsuaf.edu.cn
† These authors contributed equally to this work.

Received 22 September 2016; Editorial decision 13 January 2017; Accepted 13 January 2017

Editor: Katherine Denby, York University

Abstract

Grapevine is one of the world's most important fruit crops. European cultivated grape species have the best fruit quality but show almost no resistance to powdery mildew (PM). PM caused by *Uncinula necator* is a harmful disease that has a significant impact on the economic value of the grape crop. In this study, we examined a RING-H2-type ubiquitin ligase gene *VpRH2* that is associated with significant PM-resistance of Chinese wild-growing grape *Vitis pseudoreticulata* accession Baihe-35-1. The expression of *VpRH2* was clearly induced by *U. necator* inoculation compared with its homologous gene *VvRH2* in a PM-susceptible grapevine *V. vinifera* cv. Thompson Seedless. Using a yeast two-hybrid assay we confirmed that VpRH2 interacted with VpGRP2A, a glycine-rich RNA-binding protein. The degradation of VpGRP2A was inhibited by treatment with the proteasome inhibitor MG132 while VpRH2 did not promote the degradation of VpGRP2A. Instead, the transcripts of *VpRH2* were increased by over-expressing *VpGRP2A* while *VpRH2* suppressed the expression of *VpGRP2A*. Furthermore, *VpGRP2A* was down-regulated in both Baihe-35-1 and Thompson Seedless after *U. necator* inoculation. Specifically, we generated *VpRH2* overexpression transgenic lines in Thompson Seedless and found that the transgenic plants showed enhanced resistance to powdery mildew compared with the wild-type. In summary, our results indicate that VpRH2 interacts with VpGRP2A and plays a positive role in resistance to powdery mildew.

Key words: Disease resistance, E3 ubiquitin ligase, genetic transformation, glycine-rich RNA-binding protein, Grapevine, *Vitis pseudoreticulata*.

Introduction

The ubiquitin/26S proteasome system (UPS) is an important protein modification mechanism in eukaryotic cells that functions in plant growth and development, including flowering time, root growth, hormone signaling, abiotic stress, and biotic stress (Hellmann and Estelle, 2002; Devoto *et al.*, 2003; Dreher and Callis, 2007; Deb *et al.*, 2014; Lazaro *et al.*, 2015).

Abbreviations: ATL, Arabidopsis Tóxicos en Levadura; GUS, β-glucuronidase; OERH2, the transgenic Thompson Seedless cultivar with overexpression of *VpRH2*; PM, Powdery mildew; PR, pathogenesis-related; VpGRP2A, *Vitis pseudoreticulata* glycine-rich RNA-binding protein GRP2A.

UPS involves ubiquitin, ubiquitin-activating enzyme (E1), ubiquitin-conjugating enzyme (E2), ubiquitin ligase (E3), and the 26S proteasome (Haglund and Dikic, 2005; Du *et al.*, 2009). E3s have been divided into four main classes according to their domains: HECT (Homology to E6-AP C-Terminus), RING (Really Interesting New Gene)/U-box, SCF (Skp–Cullin–F-box), and APC (Anaphase-Promoting Complex) (Craig *et al.*, 2009; Vierstra, 2009; Chen and Hellmann, 2013; Duplan and Rivas, 2014; Morreale and Walden, 2016). The plant immunity system can be divided into two layers according to the type of pathogen molecules that are recognized by the plant. The first layer of defense responses is activated by pathogen-associated molecular patterns (PAMPS) and is termed the PAMP-triggered immunity (PTI) (Schwessinger and Zipfel, 2008), and the second layer is defense mediated by disease-resistance (R) proteins, and is termed effector-triggered immunity (ETI) (Jones and Dangl, 2006). Several RING proteins have been identified as having functions in immunity. In Arabidopsis, two RING-type E3s, AtRIN2 and AtRIN3 (RPM1-interacting proteins 2 and 3), enhance the RPM1- and RPS2-mediated hypersensitive response (HR) (Kawasaki *et al.*, 2005); AtRKP reduces the susceptibility to infection by Beet Severe Curly Top Virus (BSCTV) (Lai *et al.*, 2009); AtMIEL1 degrades AtMYB30 to attenuate cell death and weaken resistance to bacterial inoculation (Marino *et al.*, 2013). In pepper, *CaRING1* was found to be induced by *Xanthomonas campestris* pv *vesicatoria* infection, silencing of which resulted in reduced plant defense with lower salicylic acid levels (Lee *et al.*, 2011). An *Oryza sativa* E3, named OsAPIP6, targets an effector AvrPiz-t from *Magnaporthe oryzae* by ubiquitination to active PTI in *Nicotiana benthamiana* (Park *et al.*, 2012).

Powdery mildew caused by biotrophic pathogens of the Erysiphaceae family is one of the most widespread diseases in the world (Zabka *et al.*, 2008; Hoefle *et al.*, 2011) and negatively affects the development of grape, wheat, barley, Arabidopsis, and many ornamentals (Menzies *et al.*, 1992; Glawe, 2008). For example, approximately 76% of all fungicides used in European Union member states in 2003 were applied to grapevine in order to reduce the harmful effects of pathogens in although this crop only accounted for approximately 8.5% of the total cultivated area (Muthmann, 2007). In Arabidopsis, previous studies have demonstrated that the *MLO* loss-of-expression mutant shows enhanced resistance to PM and that transmembrane AtMLO acts as the point of cell entry for the PM fungi (Consonni *et al.*, 2006; Hückelhoven and Panstruga, 2011; Inada *et al.*, 2016). The expression of *AtPEN1*, *AtPEN2*, and *AtPEN3* inhibited the entry of PM fungi (Lipka *et al.*, 2008), and *AtRPW8.1* and *AtRPW8.2* conferred broad-spectrum resistance to various PM fungi (Xiao *et al.*, 2001; Wang *et al.*, 2007). In barley, MLOs and ROP binding protein kinase have been considered as regulating PM entry (Opalski *et al.*, 2005; Hoefle *et al.*, 2011; Hückelhoven and Panstruga, 2011). For wheat, a U-box-type ubiquitin ligase *CMPG1–V* was found to mediate the production of reactive oxidative species and the phytohormone pathway after PM infection (Zhu *et al.*, 2015). In grape studies, a *TIR-NB-LRR* gene *MrRUN1* (Resistance to *Uncinula necator*) in the North American wild grapevine species *Muscadinia rotundifolia* was found to confer enhanced resistance to powdery mildew (Feechan *et al.*, 2013) caused by *U. necator* originating in eastern and central North America (Cadle-Davidson *et al.*, 2011). In comparison with the PM-susceptible grapevine *V. vinifera* cv. Cabernet Sauvignon, reduced hyphal growth together with higher endogenous salicylic acid levels and more brown-colored epidermal cells were found in the PM-resistant grapevine *V. aestivalis* Norton after inoculation (Fung *et al.*, 2008). Several ubiquitin ligases have been studied in grape for their functions in abiotic and biotic stress responses, and two ubiquitin ligases have shown functions in abiotic stresses (Tak and Mhatre, 2013; Jiao *et al.*, 2015). Our research group has reported a RING-type E3 named VpEIRP1 from *V. pseudoreticulata* accession Baihe-35-1 that works as a positive regulator for *U. necator* inoculation by interacting with VpWRKY11 (Yu *et al.*, 2013*b*). However, there was yet no reports regarding the Arabidopsis Tóxicos en Levadura (ATL) subfamily members in grape.

The ATL subfamily is a special RING-finger E3 family that encodes proteins with the RING-H2 domain and transmembrane domain (Guzmán, 2012, 2014). Previous studies have predicted that the ATL family is comprised of 39 members in grape, 80 in *Arabidopsis thaliana*, and 121 in *Oryza sativa* (Aguilar-Hernández *et al.*, 2011). The first member of the ATL family, named *AtATL2*, was identified in *Arabidopsis thaliana* and functions as an early PAMP-responsive gene (Martínez-García *et al.*, 1996). *AtATL9* positively correlated with the basal defense response against powdery mildew (Berrocal-Lobo *et al.*, 2010). AtATL31, which interacts with Syntaxin of Plants 121 (AtSYP121), controls the formation of papilla where the powdery mildew fungus *Blumeria graminis* f. sp. *hordei* (*Bgh*) penetrates (Maekawa *et al.*, 2014). AtATL1 was found to be negatively regulated by AtEDR1, and *AtATL1* knock-down plants have increased sensitivity to infection by the powdery mildew fungus *Golovinomyces cichoracearum* strain UCSC1 (Serrano *et al.*, 2014).

Grapevine is an important fruit crop in the world because of its economic value and its health benefits to humans (Bouquet *et al.*, 2008). According to FAO statistics (http://faostat3.fao.org), in 2013 the global production of grapes was 77 181 122 t and it ranked fourth in fruit tree crops. Of particular importance, resveratrol, which has been verified to have cancer-chemopreventive, anti-oxidant, and anti-mutagen activities, is found in relatively high quantities in grapes and its product red wine (Jang *et al.*, 1997; Pandey and Rizvi, 2009). This discovery accelerated the development of the grape industry and resvertrol has been wildly researched for its benefits for human health (Baur *et al.*, 2006; Baur and Sinclair, 2006; Smoliga *et al.*, 2011; Szkudelski and Szkudelska, 2015). *Vitis vinifera* has the best fruit quality but shows almost no resistance to *U. necator* (Brewer and Milgroom, 2010; Cadle-Davidson *et al.*, 2011; Caffi *et al.*, 2011), and hence research into genes resistant to powdery mildew is an important task for genetic improvement and breeding in grape. China is one of the most important grape origin centers in the world with abundant wild grape resources, and Chinese wild *V. pseudoreticulata* accession Baihe-35-1 was selected as the target of

our research because of its resistance against several kinds of fungi, especially *U. necator* (Wang *et al.*, 1995). In order to research and use this resistance resource, our group has constructed a cDNA library from *V. pseudoreticulata* Baihe-35-1 inoculated with *U. necator* (Zhu *et al.*, 2012*a*), where several valuable genes have been studied (Li *et al.*, 2010; Xu *et al.*, 2010, 2011; Yu *et al.*, 2011, 2013*a*, 2013*b*; Zhu *et al.*, 2012*a*, 2012*b*, 2013). Here, we report a RING-H2-type *VpRH2* from the PM-inoculated Baihe-35-1 cDNA library that interacts with the Glycine-rich RNA-binding Protein VpGRP2A and plays a positive role in resistance to *U. necator*.

Materials and methods

Plant material and growth conditions

Tissues of *V. pseudoreticulata* accession Baihe-35-1, *V. vinifera* cv. Thompson Seedless and cv. Carignane were collected from the grape germplasm resources of Northwest A & F University, Yangling, Shaanxi, China (34°20′N, 108°24′E), and propagated and transplanted as previously described (Yu *et al.*, 2013*b*). The *VpRH2* ORF driven by the *CaMV 35S* promoter was cloned into the reconstructive vector pCAMBIA2301 using 3FLAG-tag (Zhou *et al.*, 2014) and named 35S-VpRH2-3Flag; this was then transferred into Thompson Seedless somatic embryos via *Agrobacterium tumefaciens*-mediated transformation for functional evaluation (Zhou *et al.*, 2014; Dai *et al.*, 2015). All cultures were maintained in growth chambers at 25 ± 1 °C under a 16-h photoperiod.

Arabidopsis thaliana plants (ecotype Columbia, Col-0) and tobacco plants (*Nicotiana tabacum* cv. NC89) were maintained in growth chambers at 25 ± 1°C under a 16-h photoperiod.

Inoculation with U. necator

The fungi were maintained on the leaves of *V. vinifera* cv. Cabernet Sauvignon. The procedure for inoculation of *U. necator* on grape leaves was as described previously (Wang *et al.*, 1995), with double-distilled water sprayed as a negative control (mock). Leaves were collected at 0, 6, 12, 24, 48, 72, 96, and 120 h after inoculation and immediately frozen in liquid nitrogen.

Grape plants were inoculated with *U. necator* and leaves were collected for 5 days post-inoculation (dpi). Trypan Blue staining was used to visualise the hyphae and chloral hydrate was used to destain (Serrano *et al.*, 2014). The samples were observed under a bright-field light microscope (Olympus CX21) (Wang *et al.*, 2007).

A TUNEL (TdT-mediated dUTP Nick-End Labeling) assay was used to test for cell death after *U. necator* inoculation (Phan *et al.*, 2011), using the TUNEL Apoptosis Assay Kit-FITC (7Sea Biotech, Shanghai, China). The PM-inoculated leaves were fixed for paraffin sectioning. After dewaxing, fluorescein isothiocyanate (FITC) was used to stain for cell death while PI (propidium iodide) was used for the cell nucleus. The samples were examined under a fluorescence microscope (Olympus BX51+DP70).

RNA extraction and quantitative RT-PCR analysis

The grape leaves harvested above were used for RNA extraction using the Omega Plant RNA Kit (Omega bio-tek, Norcross, Georgia), and first-stand cDNA was synthesized using the FastQuant RT Kit (with gDNase) (Tiangen Biotech, Beijing, China) (Yu *et al.*, 2013*b*). qRT-PCR using the BioEasy Master Mix (SYBR Green) (Bioer Technology, Hangzhou, China) was performed on a Bio-Rad IQ5 Real-Time PCR Detection System (Bio-Rad Laboratories, Hercules, CA, USA). The relative quantity of target mRNA was calculated using *VvActin7* (GenBank accession no. XM_002282480.3) as the house-keeping gene.

Extraction of genomic DNA and the cloning of the VpRH2 *promoter*

Grape leaves were collected for genomic DNA extraction as previously described (Yu *et al.*, 2013*a*). The purified grape genomic DNA was used as the template in amplification of the *VpRH2* promoter. The promoter sequence of *VpRH2* was obtained based on the predicted sequence on the Grape Genome Browser (http://www.genoscope.cns.fr/externe/GenomeBrowser/Vitis/) and analyzed with the plantCARE database (http://bioinformatics.psb.ugent.be/webtools/plantcare/html/) (Lescot *et al.*, 2002).

GUS activity assay

The promoter of *VpRH2* was cloned into the expression vector *pCAMBIA0390-GUS*, and the recombinant vector was transformed into *Agrobacterium* strain GV3101 for transient expression (Xu *et al.*, 2010). *Agrobacterium*-mediated vacuum infiltration was used to perform the transient transformation assay (Santos-Rosa *et al.*, 2008; Xu *et al.*, 2010). The grape leaves for transient expression were vacuumized for 30 min and cultivated in a 22 °C chamber for 2 d before the *U. necator* inoculation described above. At 24 h after *U. necator* inoculation, the grape leaves were collected for detection of GUS activity. Histochemical and quantitative GUS assays were performed according to the procedure of Jefferson (1987, 1988). GUS activities were measured with an Infinite 200 PRO Microplate Reader (TECAN, Switzerland).

Subcellular localization in Arabidopsis protoplasts

The ORFs of VpRH2 and VpGRP2A were cloned into pBI221-35S-GFP (Zhu *et al.*, 2013), generating the vectors pBI221-35S-VpRH2-GFP and pBI221-35S-VpGRP2A-GFP, respectively. The fusion constructs were transiently transformed into Arabidopsis protoplasts using PEG-mediated transformation assays (Yoo *et al.*, 2007), and the pBI221-35S-GFP vector was used as a positive control. Nuclear DNA was stained with DAPI (4', 6-diamidino-2-phenylindole). The different pattern markers [AtSec12 (AT2G01470), AtSYP121 (AT3G11820), AtSYP61 (AT1G28490), and AtVAMP721 (AT1G04750)] were cloned in to the pCAMBIA2300-35S-mCherry vector, generating the vectors AtSec12-mCherry, AtSYP121-mCherry, AtSYP61-mCherry, and AtVAMP721-mCherry. The green fluorescent protein (GFP) and mCherry signals were observed by confocal laser microscopy (LSM 510, Zeiss, Oberkochen, Germany).

Yeast two-hybrid assay

The Matchmaker™ Gold yeast two-hybrid system (Clontech, Mountain View, CA, USA) was used for yeast two-hybrid screening. The *VpRH2* ORF and $VpRH2^{1\text{-}227}$ (without the transmembrane domain, named VpRH2-R1) were cloned into pGBKT7 and subsequently transformed into the yeast strain Y2HGold. The yeast strains containing pGBKT7-VpRH2 and pGBKT7-VpRH2-R1 were transformed with a prey cDNA library from Baihe-35-1 leaves as described by Yu *et al.* (2013*a*). The vectors pGBKT7-Lam and pGBKT7-p53 were co-transformed with pGADT7-T, used as a negative and positive control, respectively.

The ORF of *VpGRP2A* was cloned into pGBKT7, while VpRH2 and VpRH2-R1 were cloned into pGADT7 to determine the interaction between VpRH2 and VpGRP2A. The recombinant vectors pGADT7-VpRH2 and pGADT7-VpRH2-R1 were co-transformed with pGBKT7-VpGRP2A. The transformed yeast cells were diluted and grown on SD/–Trp/–Leu/–His/–Ade/Aba/X-α-gal medium for interaction verification.

BiFC (bimolecular fluorescence complementation) assay

The ORFs of VpRH2 without the termination codon and VpGRP2A were cloned into the pSPYCE and pSPYNE vectors

(Waadt *et al.*, 2008) to generate pSPYCE-VpRH2 and pSPYNE-VpGRP2A, respectively. The recombinant plasmid pSPYCE-VpRH2 or pSPYNE-VpGRP2A were co-transformed with each other or with the respective empty vector into the Arabidopsis protoplast using PEG-mediated transformation assays (Yoo *et al.*, 2007). The *Agrobacterium* strains GV3101 carrying different plasmids were co-infiltrated into tobacco leaves and the corresponding empty vectors were used as the controls (Waadt *et al.*, 2008). A confocal laser microscopy (LSM 510, Zeiss, Oberkochen, Germany) was used to observe the yellow fluorescent protein (YFP) signals.

The relationship between VpRH2 and VpGRP2A at the protein and transcriptional levels

The degradation of VpRH2 and VpGRP2A in tobacco was performed as previously described (Bueso *et al.*, 2014). The ORF of VpGRP2A driven by the *CaMV 35S* promoter was cloned into the pCAMBIA2300-GFP vector. *Agrobacterium* carrying 35S-VpGRP2A-GFP or 35S-VpRH2-3Flag was infiltrated into tobacco leaves and cultivated for 48 h at 22 °C, then the leaves were treated with or without 50 μM MG132 for 12 h before harvest. In order to determine the protein level interaction between VpRH2 and VpGRP2A, different ratios of *Agrobacterium* carrying 35S-VpRH2-3Flag and 35S-VpGRP2A-GFP were mixed and infiltrated into the tobacco leaves as described by Liu *et al.* (2010). The co-infiltrated tobacco leaves were cultured for 72 h at 22 °C and then immediately frozen in liquid nitrogen. Leaf samples were collected for protein extraction by the TCA-acetone method (Wang *et al.*, 2006) and used for western blot analysis. To test the relationship between *VpRH2* and *VpGRP2A* at the transcriptional level, their promoters were used to replace *CaMV 35S*, named P_{VpRH2}-VpRH2-3Flag and $P_{VpGRP2A}$-VpGRP2A-GFP, respectively. The different combinations of recombinant vectors and empty vectors were transient-transformed into tobacco and grape leaves. The leaves were treated as described above and RNA was extracted for qRT-PCR analysis.

Transmission electron microscopy

Experiments were performed on 15-d-old leaves of OERH2 and wild-type grape plants (Alonso-Villaverde *et al.*, 2011). Samples were first fixed using 4% glutaraldehyde, then rinsed in PBS buffer and post-fixed in osmic acid for 2 h. Samples were cleaned using the PBS buffer and dehydrated using an ethanol series from low to high concentration, and finally white resin was used for embedding. Semi-thin (1 μm) sections were stained with Toluidine Blue and were observed under a bright-field light microscope (Olympus CX21), while ultra-thin (90 nm) sections were examined under a TEM (Hitachi HT7700) (Trouvelot *et al.*, 2008).

Results

Isolation and characterization of VpRH2

We initially obtained an EST sequence (GenBank accession no. GR883881), which had a predicted RING-H2 domain, from the cDNA library of *V. pseudoreticulata* accession Baihe-35-1 inoculated with *U. necator*. The full-length cDNA sequences were cloned by RACE and named *VpRH2* (GenBank accession no. KU296022), which was the homologous gene of *ATL20* in *V. vinifera*. *VpRH2* was predicted to be located on chromosome 2 using the Grape Genome Browser (http://www.genoscope.cns.fr/externe/GenomeBrowser/Vitis/) (Fig. 1A). The ORF of *VpRH2* was 1164 bp long and encoded 387 amino acids, with a RING-H2 domain (residues 314–355) at the C-terminus and a transmembrane motif (residues 233–255) determined by the SMART program (http://smart.embl-heidelberg.de/) (Fig. 1B, C). Using clustering analysis in the *V. vinifera* ATL subfamily indicated that *VpRH2* along with its closest genes *VvATL20*, *VvATL21*, and *VvATL21A*, belonged to the second clade, while others belonged to the first clade (Fig. 1D). VpRH2 shared 93.02% amino acid identity with VvRH2, and the aspartic residue 154 in VpRH2 is an insertion mutation compared to VvRH2 (see Supplementary Fig. S1 at *JXB* online).

RH2 showed differential expression levels upon U. necator *inoculation*

To understand the expression pattern of *RH2* upon PM infection, leaves of Baihe-35-1 and Thompson Seedless were inoculated with *U. necator*. The expression of *RH2* in the mock controls showed a similar trend in both grapes, with a dip in expression at 6 and 12 hpi (hours post-inoculation) compared to the other time points (Fig. 2A, B). In PM-resistant Baihe-35-1, the expression of *VpRH2* began to increase at 12 hpi, with more than a 3-fold greater increase than in the control treatment, maintaining a high level until 72 hpi, and then gradually recovering to the normal level (Fig. 2A). By contrast, *VvRH2* from the PM-susceptible Thompson Seedless grape showed a downward trend to reach a minimum value at 72 hpi, and then expression was restored at 96 hpi (Fig. 2B).

RH2 *promoter activity showed differences in resistant and susceptible grapes in response to* U. necator

The above results showed that the expression of *RH2* had an opposite response in Baihe-35-1 and Thompson Seedless after *U. necator* infection. In order to examine the different expression patterns of *VpRH2* and *VvRH2* in response to PM, we analyzed the promoter sequences of *RH2* in the two grape genotypes. In Baihe-35-1, a 1547-bp promoter of *VpRH2* was obtained, which was predicted on Chr2 (see Supplementary Fig. S2) (GenBank accession no. KU206024). Using PlantCARE, we found some defense-related elements in the promoter of *VpRH2*, including a TCA-element, two TC-rich repeats, a TGACG-motif, and two W-box elements (Supplementary Fig. S2). Comparing with the 1604-bp promoter of *VvRH2* in Thompson Seedless, three positions of the sequences were deletion mutations, and one was an insertion mutation in the promoter of *VpRH2* (Supplementary Fig. S3). The *VvRH2* promoter lacks a TGACG-motif, a TC-rich repeat, and an ERE compared to the *VpRH2* promoter, which lacks two HSEs (Fig. 2C).

To test whether the activity of the *VpRH2* and *VvRH2* promoters were induced by powdery mildew, a histochemical assay was conducted (Fig. 2D). The negative control (only *GUS* without the promoter) showed almost no expression and no change between inoculation with or without *U. necator*, and the positive control (*35S-GUS*) also showed no change but with a strong expression in both treatments. The GUS activity under the promoter of *VpRH2* with *U. necator* infection was increased more than that in the mock treatment, while the *VvRH2* promoter was decreased more than that in

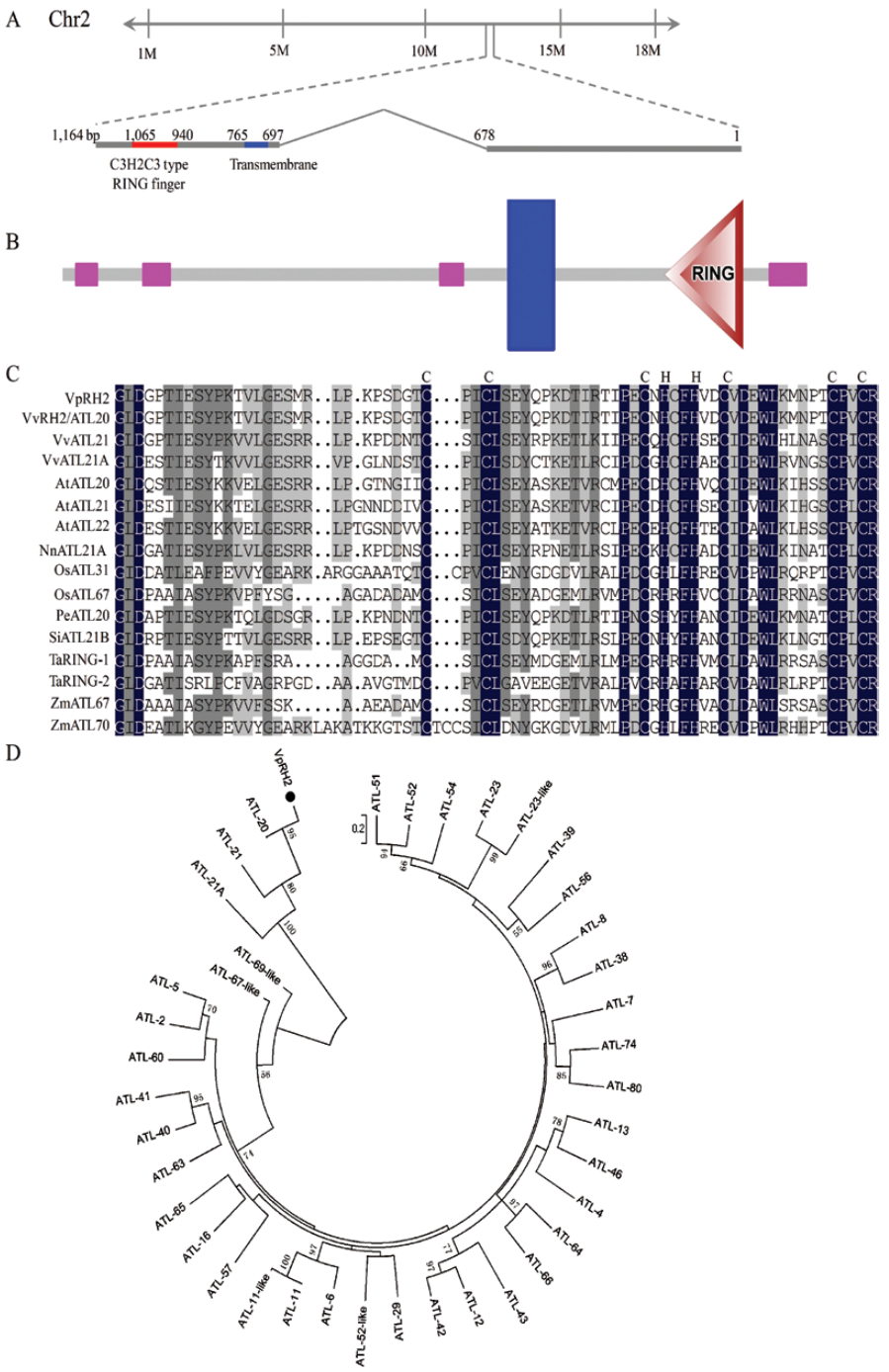

Fig. 1. Sequence analysis of the RING-H2-type ubiquitin ligase gene *VpRH2* isolated from Chinese wild *Vitis pseudoreticulata*. (A) Chromosomal location of *VpRH2*. *VpRH2* was located on the antisense strand of chromosome 2 of European grape, which is represented by the line at the top. In the detailed illustration below, the intron is represented by the broken line, the sequences 697 to 765 code the transmembrane domain, while 940 to 1065 code for the RING-H2 motif. (B) Diagram of the structure of the full-length VpRH2 protein. The line represents the amino acid sequence, on which the large rectangle is the transmembrane domain, the triangle is the RING-H2 motif, and the small rectangles are low-complexity regions. (C) Alignment of the VpRH2 RING-H2 domain with its homologs from different species: *Vitis vinifera* RING-H2 finger protein ATL20 (GenBank accession no. XM_002265958, VvATL20/VvRH2); *V. vinifera* putative RING-H2 finger protein ATL21 (GenBank accession no. XM_010664685, VvATL21); *V. vinifera* putative RING-H2 finger protein ATL21A (GenBank accession no. XM_002265958, VvATL21A); *Arabidopsis thaliana* RING-H2 finger protein ATL20 (GenBank accession no. NM_102569, AtATL20); *A. thaliana* RING-H2 finger protein ATL21 (GenBank accession no. NM_850456, AtATL21); *A. thaliana* RING-H2 finger protein ATL22 (GenBank accession no. NM_565593, AtATL22); *Nelumbo nucifera* putative RING-H2 finger protein ATL21A isoform X2 (GenBank accession no. XM_010268201, NnATL21A); *Oryza sativa* RING-H2 finger protein ATL31 (Accession no. Os02g45390, OsATL31); *O. sativa* RING-H2 finger protein ATL67 (Accession no. Os06g07100, OsATL67); *Populus euphratica* RING-H2 finger protein ATL20-like (GenBank accession no. XM_011024201, PeATL20); *Sesamum indicum* putative RING-H2 finger protein ATL21B (GenBank accession no. XM_011102742, SiATL21B); *Tritivum aestivum* RING-H2-type protein (GenBank accession no. CDM81763, TaRING-1); *T. aestivum* RING-H2-type protein (GenBank accession no. CDM82187, TaRING-2); *Zea mays* RING-H2 finger protein ATL67 (GenBank accession no. XP_008650149, ZmATL67); *Z. mays* RING-H2 finger protein ATL70 (GenBank accession no. XP_008644441, ZmATL70). (D) The phylogenetic relationship between *VpRH2* and the ATL family genes in *V. vinifera* (GenBank accession numbers are in Supplementary Table S2). VpRH2 is homologous to ATL20 in *V. vinifera* and is highlighted with a black circle. The branches are assembled into two groups, and VpRH2 and its homologous genes are clustered in the second group.

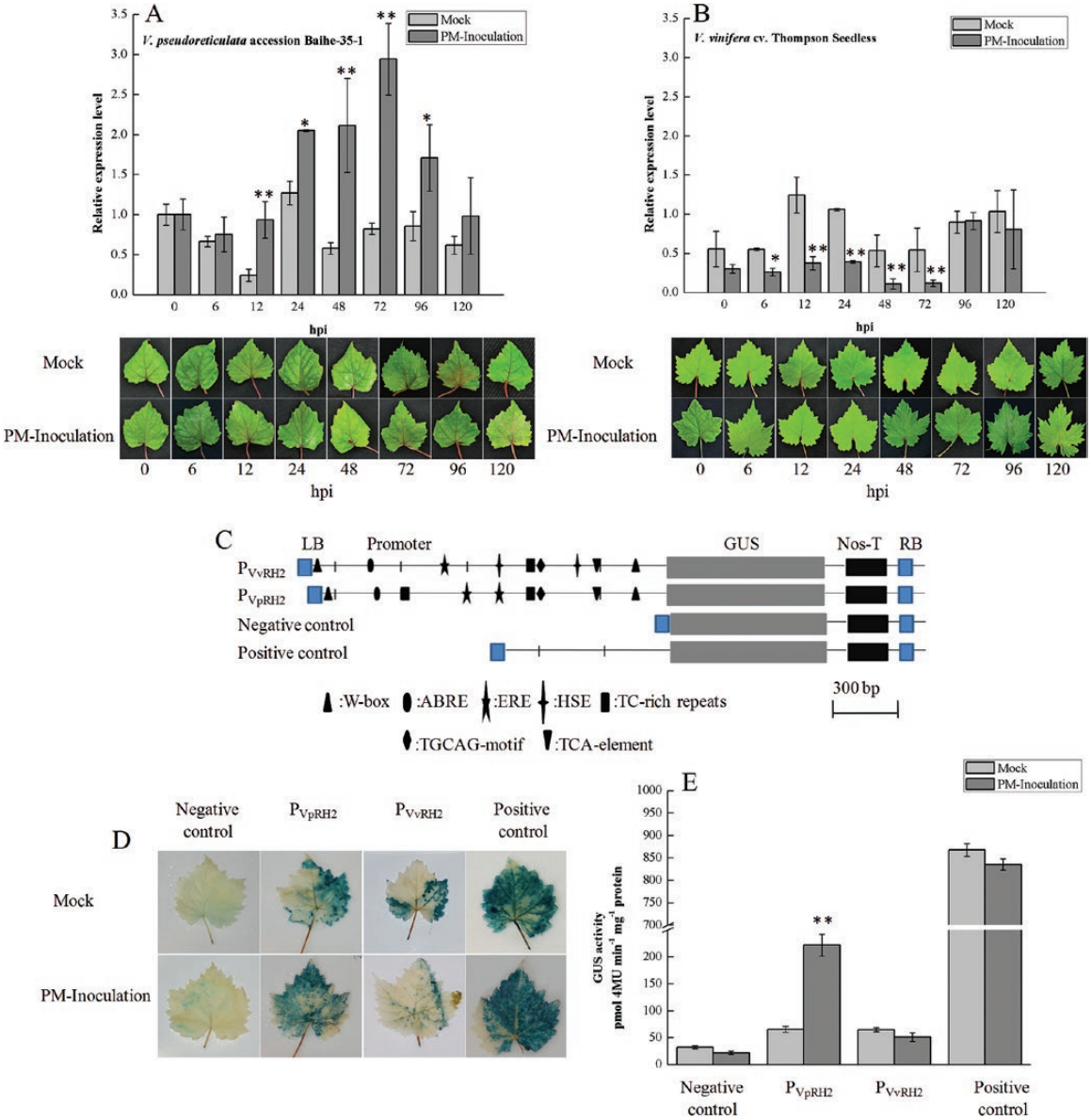

Fig. 2. Expression of the gene *RH2* and its promoter in Chinese wild *V. pseudoreticulata* and *V. vinifera* cv. Thompson Seedless in response to *U. necator*. (A, B) The expression of *RH2* was detected by qRT-PCR. Leaves of *V. pseudoreticulata* accession Baihe-35-1 (A) and *V. vinifera* cv. Thompson Seedless (B) were inoculated with *U. necator* and collected at eight time points. PM-Inoculation, powdery mildew inoculation; Mock, control inoculated with double-distilled water; hpi, hours post-inoculation. Significant differences were determined using a one-sided paired *t*-test (**$P < 0.01$, *$P < 0.05$). Expression values (±SE) of three replicates were normalized using *VvActin7* as the internal control. (C) Schematic diagram of promoter–GUS constructs. The locations of the main defense-related elements are marked on the promoters. LB, left border; *NOS-T*, Nos terminator; RB, right border; *GUS*, β-glucuronidase. The main defense-related elements are indicated by the different shapes, as explained in the key. (D) Histochemical assay for GUS expression driven by the *VpRH2* and *VvRH2* promoters under *U. necator* infection in transiently transformed grapevine leaves. The same results were obtained by three parallel treatments. Leaves were cultivated for 2 d in incubators (22 °C; photoperiod 16/8 h) before *U. necator* infection for one day. (E) Measurement of GUS activity driven by the *VpRH2* and *VvRH2* promoters under *U. necator* infection in the transiently transformed grapevine leaves. All the tests were repeated three times, and significant differences were determined using a one-sided paired *t*-test (**$P<0.01$, *$P<0.05$). Expression values (±SE) were averaged from three experiments ($n = 3$).

the mock (Fig. 2D). Quantitation of GUS activity was determined by fluorometric assays. GUS activity of the *VpRH2* promoter in pathogen-inoculated leaves was almost 3-fold higher than that in the mock treatment, and showed a highly significant difference (Fig. 2E), while the *VvRH2* promoter gave lower GUS activity than the mock after *U. necator* infection. The results from both the assays showed that compared with the *VvRH2* promoter, the promoter of *VpRH2* was obviously induced by powdery mildew, which suggests that the different expression patterns of *VpRH2* and *VvRH2* under pathogen infection may be caused by their promoters.

Subcellular localization of VpRH2

To demonstrate the subcellular localization of VpRH2, the VpRH2 over-expressing vector (pBI221-35S-VpRH2-GFP) was constructed, while free-GFP under *CaMV 35S* was used as a positive control. After transient transformation into

Arabidopsis protoplasts, pBI221-35S-VpRH2-GFP was located at the cell membrane and cytoplasm, but not in the nucleus (Fig. 3A). To further study the subcellular localization of VpRH2, pBI221-35S-VpRH2-GFP was co-expressed with several marker proteins in Arabidopsis protoplasts. Overlapping subcellular localization of VpRH2 was found by co-expressing with an endoplasmic reticulum (ER) marker AtSec12 (González *et al.*, 2005), a Golgi complex and plasma-membrane marked protein AtSYP121 (Hachez *et al.*, 2014), the TGN/EE (trans-Golgi network/early endosome) marker AtSYP61 (Hachez *et al.*, 2014), and a cell membrane and endormembrane compartments marked protein AtVAMP721 (Fendrych *et al.*, 2013; Zhang *et al.*, 2015) (Fig. 3B). The results indicated that VpRH2 was located at the cell membrane, ER, and TGN/EE.

RH2 physically interacted with GRP2A

To investigate the functional mechanisms of VpRH2 in response to powdery mildew, a yeast two-hybrid screen was performed to identify the proteins interacting with VpRH2. Thirty-six clones were obtained, and three clones encoding a glycine-rich RNA-binding protein 2A were selected as the candidate interacting protein, which was named as VpGRP2A (GenBank accession no. KU296023). After the full length of VpGRP2A was cloned, a re-transformation assay was used to verify the interaction between VpRH2 and VpGRP2A, and showed that VpRH2-R1 interacted with full-length VpGRP2A, while the ORF of VpRH2 did not (Fig. 4A, B).

To further investigate the potential relationship between VpRH2 and VpGRP2A, a bimolecular fluorescence complementation (BiFC) assay was performed. The YFP signal was detected when pSPYCE-VpRH2 was co-expressed with pSPYNE-VpGRP2A in Arabidopsis protoplasts, while no signal could be observed in control groups (Fig. 4C). The same results were detected in tobacco leaves via *A. tumefaciens*-mediated transient co-expression (Fig. 4D).

These results indicated that VpRH2 physically interacted with VpGRP2A.

VpGRP2A responded to U. necator

To verify the function of VpGRP2A in powdery mildew infection, first its sequence was analyzed. The ORF of VpGRP2A was 489 bp and encoded 162 amino acids, with a RNA-recognition motif (RRM) and a glycine-rich

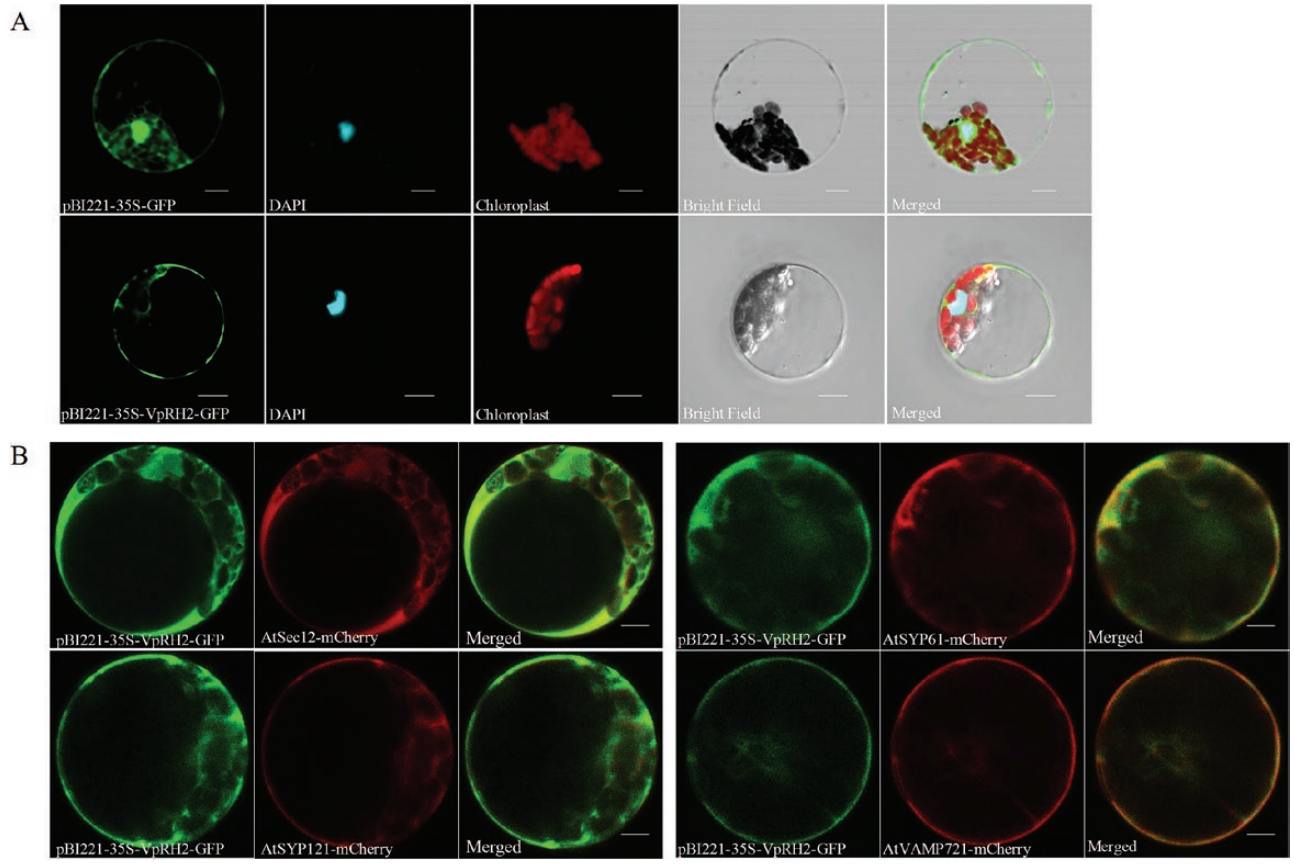

Fig. 3. (A) Subcellular localization of VpRH2 in Arabidopsis leaf protoplasts. Transient transformation of Arabidopsis protoplasts by PEG-mediated transformation assays; the GFP signal was observed by confocal laser microscopy. The nucleus was stained with DAPI. From left to right: GFP, DAPI, chloroplast, bright-field, and merged; scale bars = 10 μm. (B) Co-localization of VpRH2 with different marker proteins in Arabidopsis leaf protoplasts. Transient transformation of Arabidopsis protoplasts by PEG-mediated transformation assays. All the marker proteins were fused with mCherry and co-transformed with pBI221-35S-VpRH2-GFP. AtSec12 (AT2G01470), an endoplasmic reticulum (ER) marker; AtSYP121 (AT3G11820), marked on vesicles between the Golgi complex and the plasma membrane protein; AtSYP61 (AT1G28490), a TGN/EE (trans-Golgi network/early endosome) marker; and AtVAMP721 (AT1G04750), a cell membrane and endomembrane compartments protein. GFP and mCherry were observed by confocal laser microscopy. From left to right: GFP, mCherry and merged; scale bars = 10 μm.

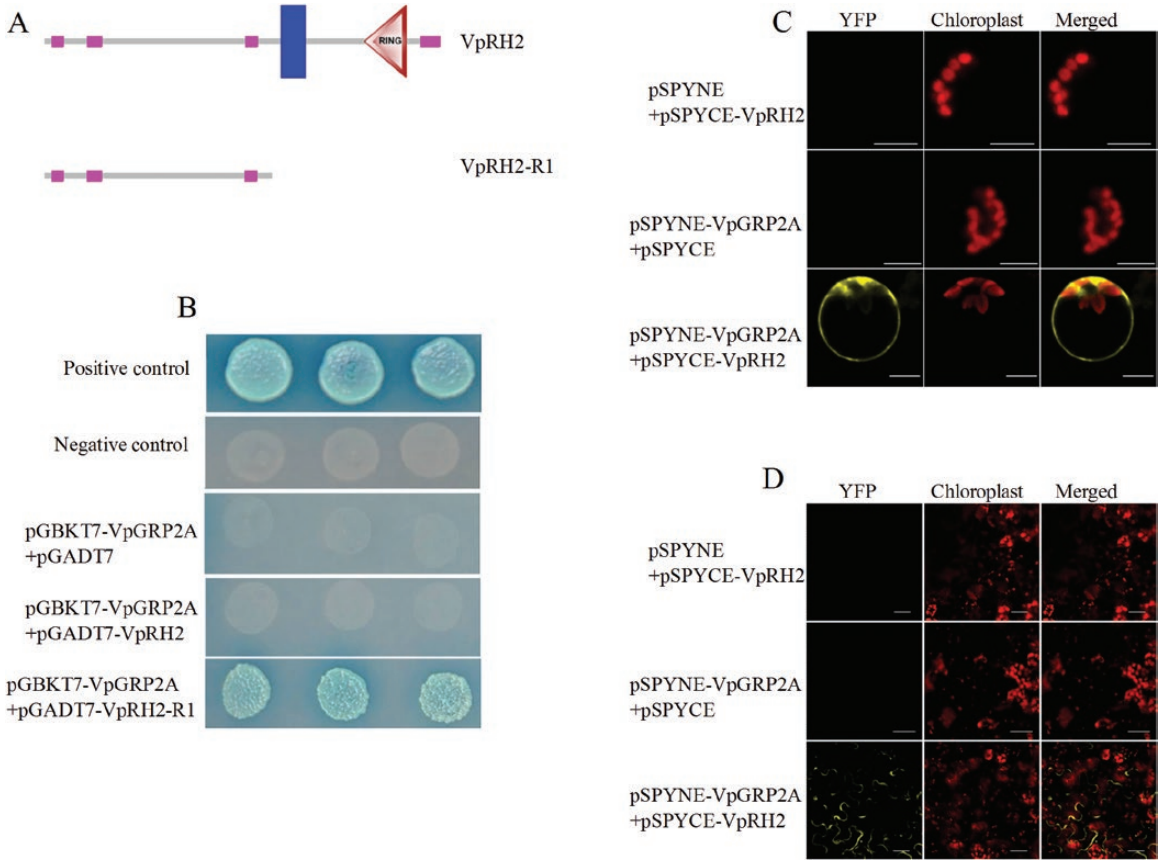

Fig. 4. (A) Schematic diagram of the VpRH2 protein and its deletant VpRH2-R1. The lines represent the amino acid sequence, the large rectangle is the transmembrane domain, the triangle is the RING-H2 motif, and the small rectangles are low-complexity regions. (B) The E3 ubiquitin ligase VpRH2 interacts with VpGRP2A in yeast. Yeast strains with pGBKT7-VpGRP2A and pGADT7-VpRH2 or pGADT7-VpRH2-R1 were grown on selective medium (SD/–Trp/–Leu/–Ade/–His). A yeast strain carrying pGBKT7-p53 and pGADT7-T was used as a positive control, with pGBKT7-Lam and pGADT7-T as a negative control. (C) The BiFC assay confirms the interaction between E3 ubiquitin ligase VpRH2 and VpGRP2A in Arabidopsis protoplasts. The plasmids carrying recombinant vectors were co-transformed into Arabidopsis protoplasts by the PEG-method; the YFP signal was observed by confocal laser microscopy. From left to right: YFP, chloroplast, and merged; scale bars = 10 μm. (D) The BiFC assay confirms the interaction between E3 ubiquitin ligase VpRH2 and VpGRP2A in tobacco leaves; the YFP signal was observed by confocal laser microscopy. From left to right: YFP, chloroplast, and merged; scale bars = 30 μm.

domain as determined by the SMART program (Fig. 5A, B). *VpGRP2A* was predicted to be located on chromosome 3 using the Grape Genome Browser (Fig. 5A). Sequence analysis showed that VpGRP2A belongs to the glycine-rich protein class Iva (Mangeon *et al.*, 2010), with a RNA recognition motif (RRM) in the N-terminal region and a glycine-rich domain arranged in $(Gly)_n$-X repeats in the C-terminus. The GRP proteins from *V. vinifera*, *Oryza sativa*, *Malus*, *Zea mays*, *Triticum aestivum*, and *Arabidopsis thaliana* were used for clustering analysis, and the results indicated that the amino acid sequence of VpGRP2A shared 100% similarity to VvGRP2A (*V. vinifera* glycine-rich RNA-binding protein2A, GenBank accession no. XM_003631610) (Fig. 5C).

To further examine its role in pathogen infection, *GRP2A* expression in Baihe-35-1 and Thompson Seedless after *U. necator* inoculation was measured by qRT-PCR. The expression of *GRP2A* in the mock was similar in the two grapes and showed an initial increase before returning to normal levels. The expression of *GRP2A* after *U. necator* inoculation also showed a similar trend in the two grapes, clearly decreasing from 6 hpi to 24 hpi comparing with the expression in the mock treatment, then returning to normal levels after 24 hpi (Fig. 5D, E). These results indicated that *VpGRP2A* responded to PM.

To study the function of VpGRP2A, its subcellular localization was determined. After transient transformation into Arabidopsis protoplasts, pBI221-35S-VpGRP2A-GFP was located at the cell membrane, cytoplasm, and nucleus (Fig. 6A). To further study the subcellular localization of VpGRP2A, pBI221-35S-VpGRP2A-GFP was co-expressed with several marker proteins in Arabidopsis protoplasts. The overlapping subcellular localization of VpGRP2A was found by co-expressing with AtSec12, AtSYP121, AtSYP61, and AtVAMP721 (Fig. 6B). These results indicated that VpGRP2A was located at the cell membrane, ER, and TGN/EE.

The relationship between VpRH2 and VpGRP2A

VpRH2 was predicted as a RING-H2-type ubiquitin ligase. We firstly tested whether VpRH2 and its interacting protein VpGRP2A were degraded by UPS. 35S-VpRH2-3Flag and 35S-VpGRP2A-GFP were transient transformed into tobacco leaves using *Agrobacterium*-mediated transformation. After being infiltrated with 50 μM MG132 (a 26S proteasome-specific

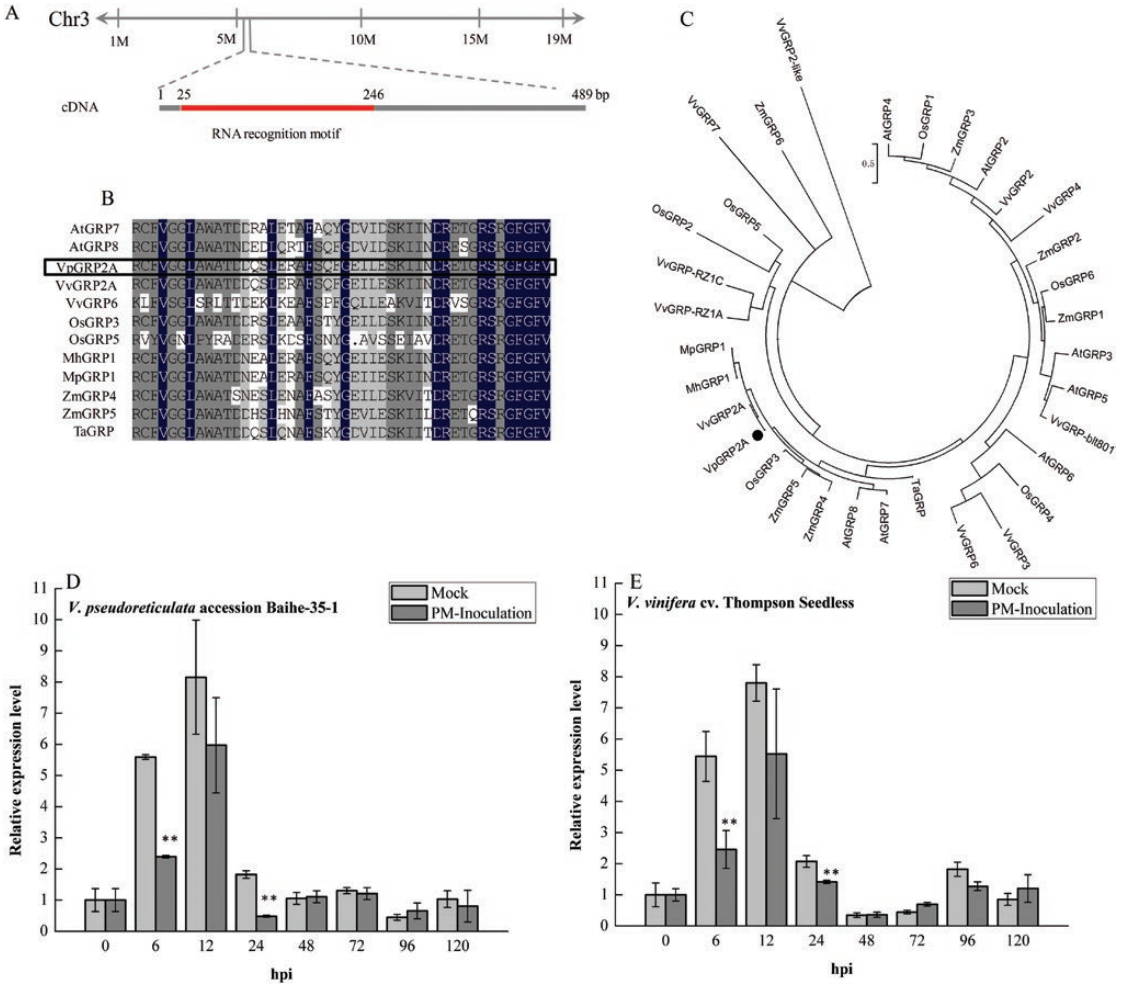

Fig. 5. Sequence and function analysis of *VpGRP2A*. (A) Chromosomal location of VpGRP2A with conserved RNA-recognition motif. VpGRP2A was located on the positive sense strand of chromosome 3 of European grape, represented by the line at the top. The detailed line below represents the nucleotide sequences, with 25 to 246 coding the RNA-recognition motif. (B, C) Alignment (B) and phylogenetic relationship (C) of the VpGRP2A RNA-recognition motif amino acid sequence with its homologs in *V. vinifera*, *Arabidopsis*, *Malus*, *Zea mays*, *Triticum aestivum*, and *Oryza sativa*. VpGRP2A is highlighted with a box in (B) and a black circle in (C). *Arabidopsis thaliana* glycine-rich RNA-binding protein 2 (GenBank accession no. NM_117459, AtGRP2); *A. thaliana* glycine-rich RNA-binding protein 3 (GenBank accession no. NM_125496.2, AtGRP3); *A. thaliana* glycine-rich RNA-binding protein 4 (GenBank accession no. NM_180298.3, AtGRP4); *A. thaliana* glycine-rich RNA-binding protein 5 (GenBank accession no. NM_106083.4, AtGRP5); *A. thaliana* glycine-rich RNA-binding protein 6 (GenBank accession no. NM_101721.3, AtGRP6); *A. thaliana* glycine-rich RNA-binding protein 7 (GenBank accession no. NM_127738.4, AtGRP7); *A. thaliana* glycine-rich RNA-binding protein 8 (GenBank accession no. NM_120087.3, AtGRP8); *Malus hupehensis* glycine-rich RNA-binding protein 1 (GenBank accession no. HQ_380209, MhGRP1); *M. prunifolia* glycine-rich RNA-binding protein 1 (GenBank accession no. HM_042682, MpGRP1); *Oryza sativa* glycine-rich RNA-binding protein 1 (Accession no. Os01g68790, OsGRP1); *O. sativa* glycine-rich RNA-binding protein 2 (Accession no. Os03g56020, OsGRP2); *O. sativa* glycine-rich RNA-binding protein 3 (Accession no. Os03g46770, OsGRP3); *O. sativa* glycine-rich RNA-binding protein 4 (Accession no. Os04g33810, OsGRP4); *O. sativa* glycine-rich RNA-binding protein 5 (Accession no. Os05g13620, OsGRP5); *O. sativa* glycine-rich RNA-binding protein 6 (Accession no. Os12g31800, OsGRP6); *Triticum aestivum* glycine-rich RNA-binding protein (GenBank accession no. AGI04359.1, TaGRP); *Zea mays* glycine-rich RNA-binding protein 1 (Accession no. GRMZM2G150521, ZmGRP1); *Z. mays* glycine-rich RNA-binding protein 2 (Accession no. GRMZM2G1311671, ZmGRP2); *Z. mays* glycine-rich RNA-binding protein 3 (Accession no. GRMZM2G042118, ZmGRP3); *Z. mays* glycine-rich RNA-binding protein 4 (Accession no. GRMZM2G165901, ZmGRP4); *Z. mays* glycine-rich RNA-binding protein 5 (Accession no. GRMZM2G080603, ZmGRP5); *Z. mays* glycine-rich RNA-binding protein 6 (Accession no. GRMZM2G001850, ZmGRP6); *Z. mays* glycine-rich RNA-binding protein 7 (Accession no. GRMZM5G874478, ZmGRP7); *Z. mays* glycine-rich RNA-binding protein 8 (Accession no. GRMZM2G082931, ZmGRP8); *Vitis vinifera* glycine-rich RNA-binding protein 2 (GenBank accession no. XM_002264859.3, VvGRP2); *V. vinifera* glycine-rich RNA-binding protein 2A (GenBank accession no. XM_003631610.2, VvGRP2A); *V. vinifera* glycine-rich RNA-binding protein 2-like (GenBank accession no. XM_002277592.3, VvGRP2-like); *V. vinifera* glycine-rich RNA-binding protein 3 (GenBank accession no. XM_002271188.3, VvGRP3); *V. vinifera* glycine-rich RNA-binding protein 4 (GenBank accession no. XM_002273962.2, VvGRP4); *V. vinifera* glycine-rich RNA-binding protein 6 (GenBank accession no. XM_002274142.2, VvGRP6); *V. vinifera* glycine-rich RNA-binding protein 7 (GenBank accession no. XM_002266977.3, VvGRP7); *V. vinifera* glycine-rich RNA-binding protein blt801 (GenBank accession no. XM_010664936.1, VvGRP-blt801); *V. vinifera* glycine-rich RNA-binding protein RZ1A (GenBank accession no. XM_010666679.1, VvGRP-RZ1A); *V. vinifera* glycine-rich RNA-binding protein RZ1C (GenBank accession no. XM_002265894.3, VvGRP-RZ1C). (D, E) Expression of *GRP2A* in response to *U. necator* in Chinese wild *V. pseudoreticulata* Baihe-35-1 (D) and *V. vinifera* cv. Thompson Seedless (E). The expression of *GRP2A* was detected by qRT-PCR. Leaves were inoculated with *U. necator* and collected at eight time points. PM inoculation, powdery mildew inoculation; Mock, control inoculated with double-distilled water; hpi, hours post-inoculation. Significant differences were determined using a one-sided paired *t*-test (***P*<0.01, **P*<0.05), expression values (±SE) of three experiments were normalized using *VvActin7* as the internal control.

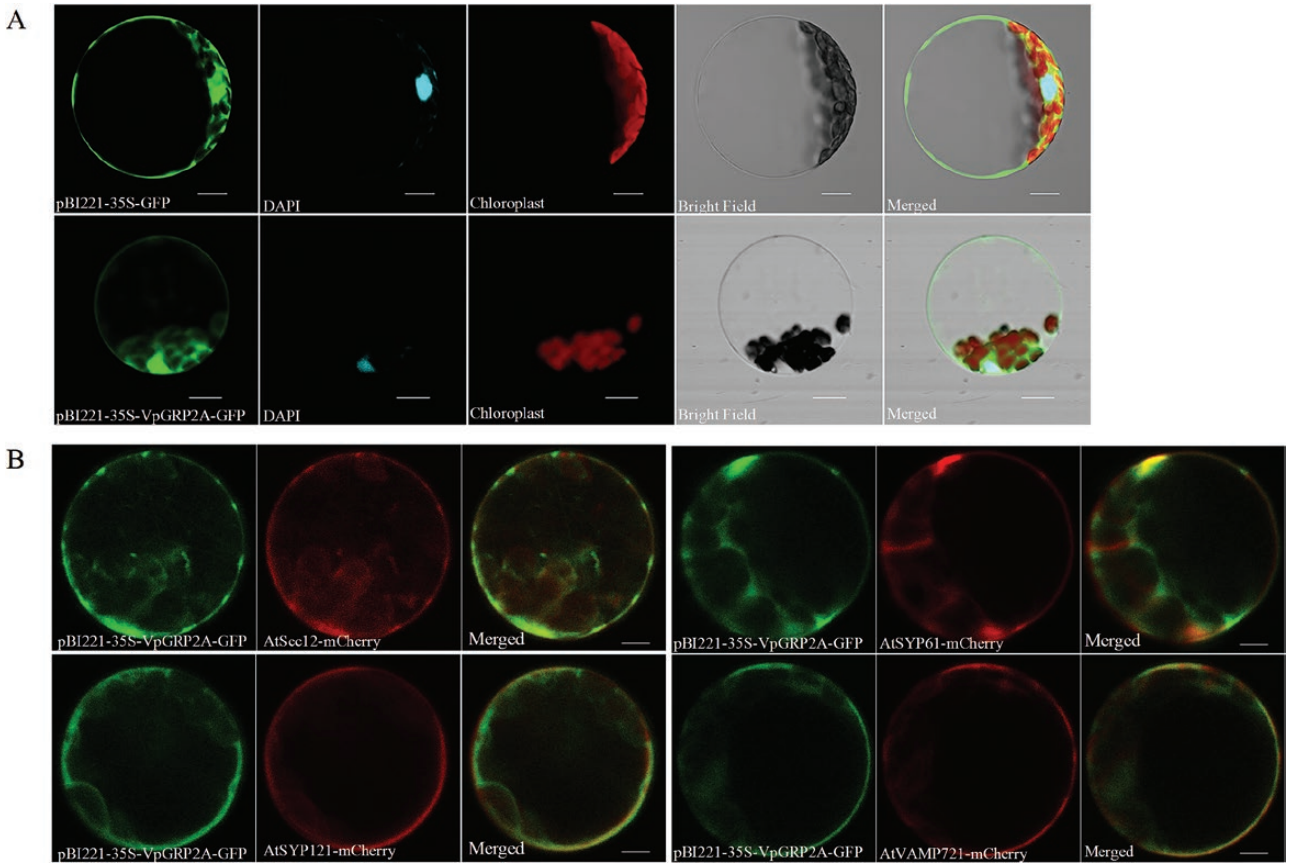

Fig. 6. (A) Subcellular localization of VpGRP2A in Arabidopsis leaf protoplasts. Transient transformation of Arabidopsis protoplasts by PEG-mediated transformation assays; the GFP signal was observed by confocal laser microscopy. The nucleus was stained with DAPI. From left to right: GFP, DAPI, chloroplast, bright-field, and merged; scale bars = 10 μm. (B) Co-localization of VpGRP2A with different marker proteins in Arabidopsis leaf protoplasts. Transient transformation of *Arabidopsis* protoplasts by PEG-mediated transformation assays. All the marker proteins were fused with mCherry and co-transformed with pBI221-35S-VpGRP2A-GFP. GFP and mCherry were observed by confocal laser microscopy. From left to right: GFP, mCherry, and merged; scale bars = 10 μm.

protease inhibitor) for 12 h, the leaves were collected and the total protein was extracted; leaves without MG132 infiltration were used as the mock treatment. The protein level of VpRH2 showed an accumulation trend, while VpGRP2A showed a similar trend (Fig. 7A). These results showed that the degradation of VpRH2 and VpGRP2A was via UPS in tobacco.

To test the interaction of VpRH2 and VpGRP2A at the protein level, different ratios of co-expression of 35S-VpRH2-3Flag and 35S-VpGRP2A-GFP were co-infiltrated in the tobacco leaves. In this assay, the protein expression of 35S-VpRH2-3Flag (the exposure time of 35S-VpRH2-3Flag protein was 255.5 s) fell far lower than that of 35S-VpGRP2A-GFP (the exposure time of 35S-VpGRP2A protein was 10.0 s). Western blot analysis indicated that when the infiltration ratio of VpRH2-3Flag increased, the protein level of VpGRP2A-GFP did not obviously declined (Fig. 7B).

These results suggested that the abundance of VpGRP2A protein was regulated by UPS, but the degradation was not observably promoted by VpRH2.

VpGRP2A enhanced the expression of VpRH2*, but VpRH2 suppressed the expression of* VpGRP2A

As VpGRP2A was predicted as a RNA-binding protein, we tested the relationship between *VpRH2* and *VpGRP2A* at the transcriptional level. P_{VpRH2}-VpRH2-3Flag and $P_{VpGRP2A}$-VpGRP2A-GFP were co-expressed into tobacco leaves and empty vectors were used as the control. At the transcriptional level, *VpGRP2A* showed a high expression level while *VpRH2* showed a low expression (Fig. 8A, B). However, when *VpRH2* was co-infiltrated with *VpGRP2A*, the expression of *VpRH2* showed an increased trend while the expression of *VpGRP2A* was inhibited. So *VpGRP2A* enhanced the expression of *VpRH2* but *VpRH2* suppressed the expression of *VpGRP2A*.

To investigate the relationship between *VpRH2* and *VpGRP2A* in grape, P_{VpRH2}-VpRH2-3Flag and $P_{VpGRP2A}$-VpGRP2A-GFP vectors were transient expressed in Baihe-35-1 and Thompson Seedless leaves. Over-expression of *VpRH2* reduced the expression of *GRP2A* in both grapes, but over-expression of *VpGRP2A* increased the expression of *RH2* (Fig. 8C). After *U. necator* inoculation, the influence of *VpRH2* on *VpGRP2A* expression showed a similar trend as in the no-infection treatment, and the change in Baihe-35-1 was more observable than in Thompson Seedless (Fig. 8D). In summary, *VpRH2* showed a similar influence on *VpGRP2A* in PM-resistant and PM-susceptible grapes, and the effect in the PM-resistant grape was more observable than that in the PM-susceptible gape after *U. necator* inoculation.

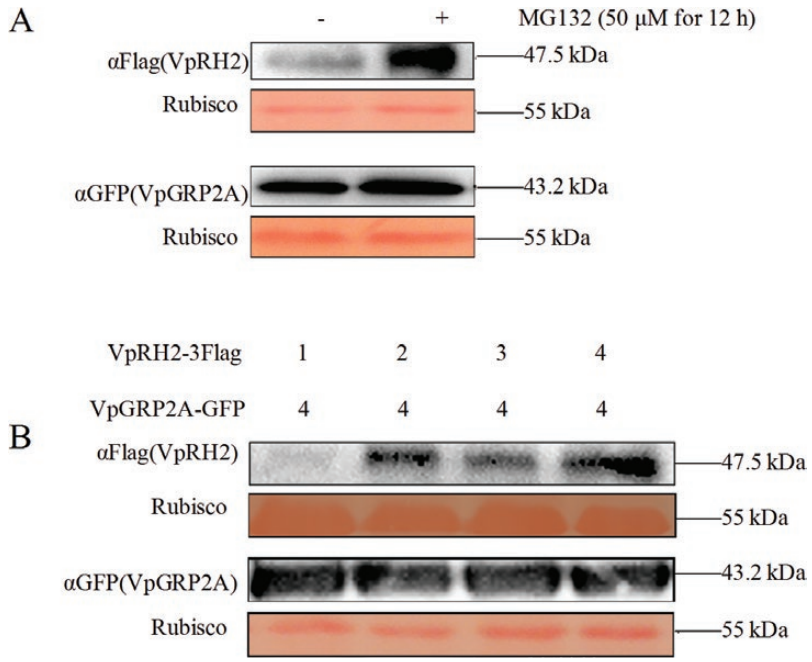

Fig. 7. The relationship between VpRH2 and VpGRP2A at the protein level. (A) VpRH2 and VpGRP2A were degraded via 26S-Proteasome in tobacco. 35S-VpRH2-3Flag and 35S-VpGRP2A-GFP were transiently expressed in tobacco and treated with or without 50 μM MG132 for 12 h. Western blotting showed the abundance of 35S-VpRH2-3Flag and 35S-VpGRP2A-GFP; molecular mass is indicated on the right: 35S-VpRH2-3Flag 47.5 kDa, and 35S-VpGRP2A-GFP 43.2 kDa. Ponceau S staining confirmed equal loading. (B) Protein-level detection of VpGRP2A by co-expression with VpRH2. Keeping the protein level of 35S-VpGRP2A-GFP invariable and increasing the protein level of 35S-VpRH2-3Flag in the tobacco leaves, western blotting showed the abundance of 35S-VpRH2-3Flag and 35S-VpGRP2A-GFP. Molecular mass is indicated on the right: 35S-VpRH2-3Flag 47.5 kDa, and 35S-VpGRP2A-GFP 43.2 kDa. Ponceau S staining confirmed equal loading.

Overexpression of VpRH2 enhanced disease resistance in Thompson Seedless grapes

Twelve plant lines (named OERH2-1 to OERH2-12) (see Supplementary Fig. S4A) were regenerated from transformed somatic embryos for further analysis. For PCR testing, a band of 1148 bp was amplified from all plants except OERH2-5, as shown in Supplementary Fig. S4B. Ten plants were verified as positive transgenic grapevines with a band of 47.5 kDa after western blot analysis (Supplementary Fig. S4C). In the negative control, no bands were found in either the DNA or the protein sample. Three lines were selected for examination of their PM response. The expression of *RH2* was analyzed in these three transgenic grapes and in the wild-type, and it was found that in the transgenic plants *VpRH2* showed a more than 12 000-fold increase (Supplementary Fig. S4D).

To further test the mechanism of PM resistance, OERH2 plants (OERH-1, OERH-3, and OERH-7) were inoculated with *U. necator*, with wild-type Thompson Seedless used as the negative control (Fig. 9A). In the transgenic OERH2 grapes, the expression of *GRP2A* in the control treatment showed a similar trend to the wild-type grapes, and *GRP2A* was down-regulated in PM-treated leaves at 6 hpi to 96 hpi comparing with the mock treatment (Fig. 9B).

Using the Trypan Blue microscopic visualization, areas of cell death and fungal hyphae can be observed under a light microscope (Serrano *et al.*, 2014). The OERH2 grape leaves showed an inhibition of the spread of hyphae at 4 dpi and areas of cell death at 5 dpi when compared with wild-type grape leaves, as shown in Fig. 9C, which indicated that over-expression of *VpRH2* could enhance the resistance to *U. necator*. In order to verify that cell death was caused by *U. necator* infection, the TUNEL assay was used to test the grape leaves. In this assay, the leaves of wild-type grape showed almost no fluorescence, while there were strong fluorescent signals in the OERH2 plants (Fig. 9D). The number of conidiophores in the transgenic OERH2 and wild-type Thompson Seedless grapes was determined in order to measure fungal reproduction. All three transgenic plants showed a clearly reduced number, with the OERH2-1 and OERH2-7 lines showing a significant difference and the OERH2-3 line showing a highly significant difference when compared with the wild-type (Fig. 9E).

These results showed that the over-expression of *VpRH2* can enhance PM resistance in grapes. In addition, the transcript levels of defense-related genes were detected by qRT-PCR, and *NPR1*, *PR1*, *PR10.1*, and *BAK1* were all higher in the transgenic plants than in the wild-type Thompson Seedless after *U. necator* inoculation (Fig. 10A, B, D, E). For *PR3*, expression was induced by *U. necator* but there was almost no difference between the transgenic grapes and the wild-type Thompson Seedless (Fig. 10C).

Overexpression of VpRH2 promoted early growth in transgenic Thompson Seedless grapes

As well as enhanced resistance to powdery mildew, the OERH2 plants displayed an accelerated growth phenotype. After culture for 2 months in planting medium, OERH2-positive plants showed an increased growth phenotype compared

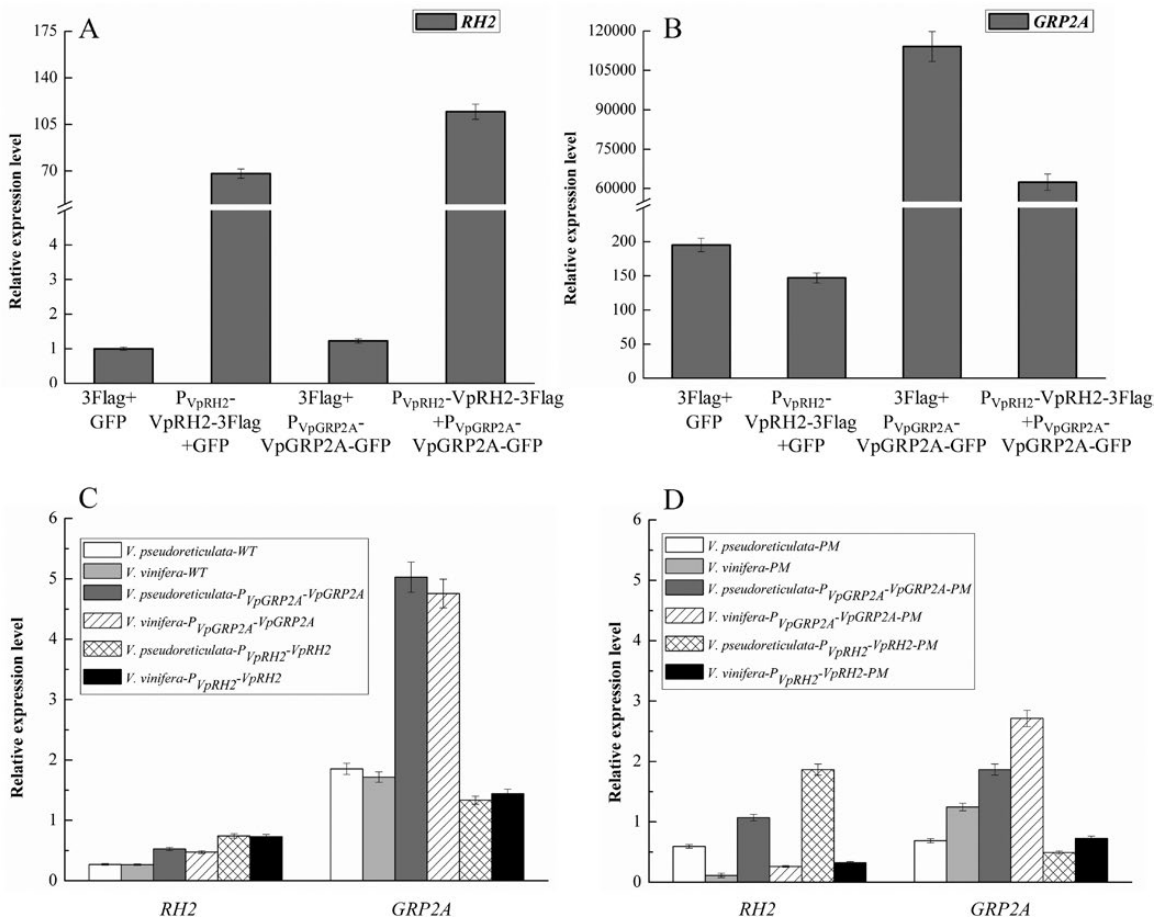

Fig. 8. The relationship between *VpRH2* and *VpGRP2A* protein at the transcriptional level. (A, B) Transcriptional level of *VpRH2* (A) and *VpGRP2A* (B) and their respective homologous genes in the follow treatments: 3Flag+GFP, P_{VpRH2}-VpRH2-3Flag+GFP, 3Flag+$P_{VpGRP2A}$-VpGRP2A-GFP, and P_{VpRH2}-VpRH2-3Flag+ $P_{VpGRP2A}$-VpGRP2A-GFP. Expression values (±SE) of three experiments were normalized using *NtActin* as the internal control. (C, D) Expression of *RH2* and *GRP2A* in response to *U. necator* in Chinese wild *V. pseudoreticulata* Baihe-35-1 and *V. vinifera* cv. Thompson Seedless. The expression of *RH2* and *GRP2A* was detected by qRT-PCR. The expression of *RH2* and *GRP2A* in the mock treatment (C) and *U. necator* treatment (D) in grape leaves were analyzed by qRT-PCR, and the transient expression was obtained by *Agrobacterium*-mediated transient expression with different vectors. Expression values (±SE) of three experiments were normalized using *VvActin7* as the internal control.

to non-transgenic plants (Fig. 11A). After transferring the grapevines into the greenhouse, the OERH2 plants showed accelerated growth after cultivation for 15 and 30 d, with auxetic leaves and increased internodal length (Fig. 11D).

The cellular organization of grape leaves was examined using semi-thin sections observed under a 40× microscope. Cells in the OERH2 plants were larger and longer than those in the wild-type, and a unique structure was found in some of the spongy parenchyma cells of the OERH2 plants (Fig. 11E). The presence of these structures was confirmed in the ultra-thin sections, where they were found in the large central vacuole and tonoplast and looked like polymerized macromolecules (Fig. 11E).

These results showed that overexpression of *VpRH2* in the Thompson Seedless grape can accelerate plant growth, which is accompanied by the presence of polymerized macromolecules in the spongy parenchyma.

Discussion

The UPS has been shown to provide regulation in various processes of plant immunity (Trujillo and Shirasu, 2010). For example, PUB22, PUB23, and PUB24 were shown to be negative regulators in PAMP-triggered immunity (PTI) (Trujillo *et al.*, 2008), and PUB22 was found to degrade EXO70B2 to weaken PTI (Stegmann *et al.*, 2012). PUB12 and PUB13 were found to ubiquitinate and promote FLS2 degradation to reduce PTI in Arabidopsis (Lu *et al.*, 2011). The important role of ubiquitination in plant immunity may be because pathogens influence the host UPS (Marino *et al.*, 2012, 2013). In this study, it is shown that *VpRH2*, a predicted RING-H2-type ubiquitin ligase, shares induced expression after *U. necator* inoculation. The overexpression of *VpRH2* in grapes resulted in enhanced resistance to PM, and accordingly *VpRH2* functions as a positive regulator in plant immunity.

RING-type ubiquitin ligases have a distinct zinc finger domain and are divided into two major types, RING-HC (C3HC4) and RING-H2 (C3H2C3) (Stone *et al.*, 2005; Guzmán, 2014). VpRH2 from PM-resistant grape Baihe-35-1 was predicted as a RING-H2-type ATL20 ubiquitin ligase (Fig. 1A, B). In previous studies, 80 ATL subfamily members in Arabidopsis and 121 in *Oryza sativa* were identified and clustered into 14 groups (a–n) (Serrano *et al.*, 2006)

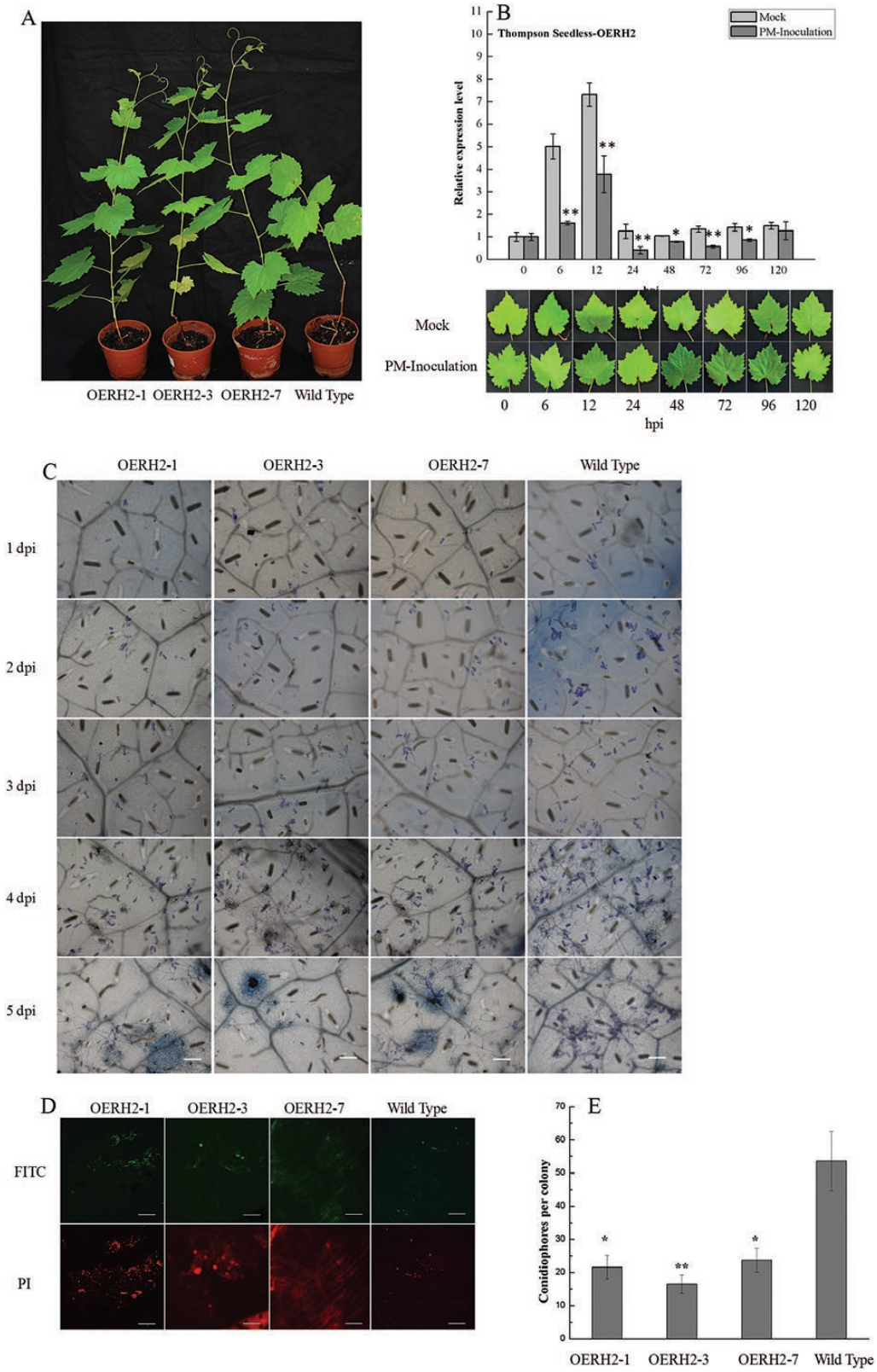

Fig. 9. Overexpression of *VpRH2* in Thompson Seedless enhanced the resistance to *U. necator*. (A) Transgenic and wild-type grapes used in this experiment. (B) The expression of *GRP2A* was detected by qRT-PCR. Leaves of transgenic Thompson Seedless were inoculated with *U. necator* and collected at eight time points. PM inoculation, powdery mildew inoculation; Mock, control inoculated with double-distilled water; hpi, hours post-inoculation. Significant differences were determined using a one-sided paired *t*-test (**P<0.01, *P<0.05). Expression values (±SE) of three experiments were normalized using *VvActin7* as the internal control. (C) Transgenic grapes showed enhanced *U. necator* resistance. The images are microscopic visualizations of hyphal development 5 d after inoculation. Leaves were stained with Trypan blue; scale bars = 100 μm. (D) TUNEL- or PI-labeled signals detected in transgenic and wild-type grapes leaves. The leaves were inoculated with *U. necator* and examined after 5 d; scale bars = 100 μm. (E) Quantification of *U. necator* growth on grape leaves as determined by counting the number of conidiophores per colony at 5 d post-inoculation. The means (±SE) were based on at least 20 replications, and Significant differences were determined using a one-sided paired *t*-test (**P<0.01, *P<0.05).

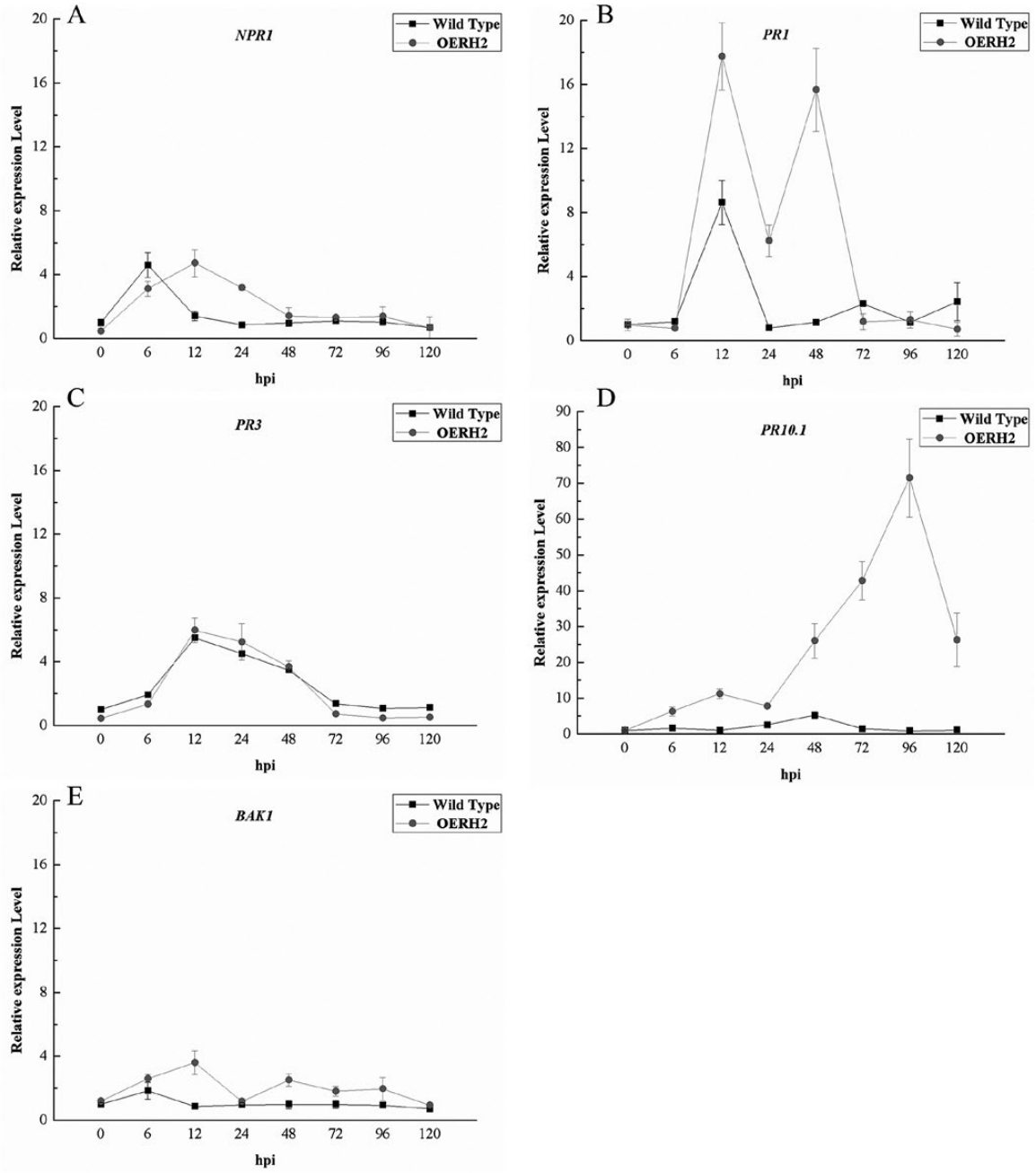

Fig. 10. qRT-PCR analysis of defense-related genes in wild-type and transgenic plants after *U. necator* inoculation. Expression of *NPR1* (A), *PR1* (B), *PR3* (C), *PR10.1* (D) and *BAK1* (E) was detected by qRT-PCR. Leaves of wild-type and transgenic OERH2 *V. vinifera* cv. Thompson Seedless were inoculated with *U. necator* and collected at eight time points; hpi, hours post-inoculation. Expression values (±SE) of three experiments were normalized using *VvActin7* as the internal control.

with VpRH2 being classified into group k, the proteins in this group showing sequence similarities in Arabidopsis and *Oryza sativa*. However, whilst group k in Arabidopsis contains no intron, VpRH2 has one intron (Fig. 1A). A RING-HC ubiquitin ligase gene *EIRP1*, which positively regulates plant immunity by interacting with VpWRKY11 has previously been studied by our research group (Yu *et al.*, 2013*b*). Comparing to EIRP1 from the same cDNA library, *VpRH2* was also verified to participate in the plant response to *U. necator* by causing cell death (Fig. 9C, D).

In our results, the ATL family gene *VpRH2* influenced the immune response and plant development. Another ATL family gene, *ATL1*, was previously shown to function in the immune response and plant development in Arabidopsis (Serrano *et al.*, 2014). Overexpressed *ATL1* induced severe growth inhibition in transgenic Arabidopsis plants, and *VpRH2*-overexpressing transgenic Thompson Seedless plants showed increased development compared with wild-type plants (Fig. 11B, C). Although they belong to the same family, *VpRH2* and *ATL1* produce completely different responses in plant development, possibly because *VpRH2* belongs to group k in the second clade, while *ATL1* belongs to group i in the first clade (Serrano *et al.*, 2006). Knock-down of *ATL1* leads to hyper-susceptibility to powdery mildew infection in

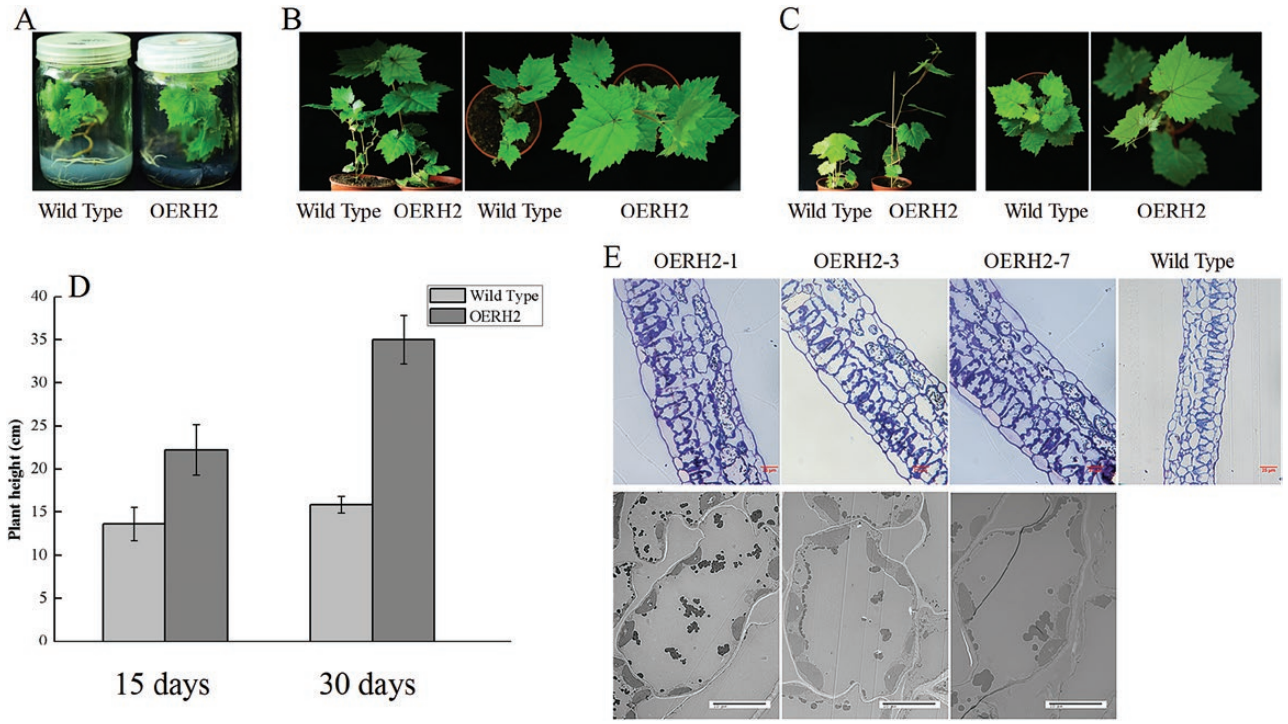

Fig. 11. Phenotype analysis of 12 selected OERH2 transgenic Thompson Seedless lines. (A) Plants formed on planting medium for 2 months. Left is the wild-type Thompson Seedless, and right is the transgenic plant. (B) Plants grown on a feeding block for 15 d. Left is the wild-type Thompson Seedless, and right is the transgenic plant in each image. (C) Plants grown on a feeding block for 30 d. Left is the wild-type Thompson Seedless, and right is the transgenic plant in each image. (D) The effects of transgenic OERH2 in *Vitis vinifera* cv. Thompson Seedless on plant height. The means (±SE) were based on at least 10 replications. (E) Top: semi-thin sections of wild-type and transgenic Thompson Seedless leaves; scale bars = 25 μm. Bottom: ultra-thin sections of transgenic Thompson Seedless leaves; scale bars = 10 μm.

transgenic Arabidopsis plants (Serrano *et al.*, 2014), and cell death was increased as a means to inhibit the spread of hyphae in *VpRH2* over-expressing transgenic Thompson Seedless plants (Fig. 9C, D). Above all, despite inverse influences on plant development, the two genes show the same positive effect with regards to the response to powdery mildew.

In plants, several GRPs had been reported to be regulated by abiotic and biotic stresses. For example, two *Malus* GRPs hve been shown to function in salt and drought stresses (Wang *et al.*, 2010; Tan *et al.*, 2014). OsGRP1, OsGRP4, and OsGRP6 increased cold tolerance when heterogenetically expressed in Arabidopsis (Kim *et al.*, 2010). However, no GRPs had been reported in grapes. In yeast, VpGRP2A interacts with VpRH2-R1 but it does not interact with VpRH2. According to the Matchmaker™ Gold yeast two-hybrid system and previous studies, the transmembrane proteins may aggregate, misfold, or otherwise be unable to interact with partner proteins, when targeted to the aqueous nucleoplasm (Paumi *et al.*, 2007). In our results, VpRH2 located in the cell membrane in Arabidopsis protoplasts and may also locate on the cell membrane or be secreted out in the yeast cells, so the transmembrane motif of VpRH2 may be the reason VpGRP2A interacts with VpRH2-R1 (VpRH2 no-transmembrane mutation) but not with VpRH2. And the different internal systems between yeast and plants cells may also influence the interaction between VpRH2 and VpGRP2A. VpGRP2A, which showed a 100% similarity to VvGRP2A in Thompson Seedless (Fig. 5C), is conserved in grape. VpGRP2A has high homology to glycine-rich RNA-binding protein7 (AtGRP7) in Arabidopsis (Fig. 5C), which has been more thoroughly studied than other reported GRPs (Fu *et al.*, 2007; Kim *et al.*, 2007, 2008; Schöning *et al.*, 2007; Jeong *et al.*, 2011; Kwak *et al.*, 2011). AtGRP7 functions as a component of a circadian regulator and plays a role in the nucleus (Heintzen *et al.*, 1997). From our subcellular study, VpGR2A has nuclear localization (Fig. 6A), similar to AtGRP7 (Heintzen *et al.*, 1997). We predict that VpGRP2A may also play roles in the nucleus. In our study, *RH2* in the mock treatment showed a decrease in expression at 6 and 12 hpi compared with other time points (Fig. 2A, B), while expression of *GRP2A* in the control showed a higher expression at 6 and 12 hpi compared with other time points (Fig. 5D, E), and the reason may be due to the grape GRP2A playing a similar role to Arabidopsis AtGRP7 in circadian regulation. AtGRP7 was found to interact with FLS2 and EFR (Nicaise *et al.*, 2013). In our study, we showed that VpRH2 physically associated with VpGRP2A on the cytoplasm and cell membrane (Fig. 4C, D), where AtGRP7 interacts with FLS2 and EFR. As well as the interaction with AtGRP7, FLS2 and EFR were found to interact with BAK1, which is associated with developmental regulation and PRR-dependent signaling (Chinchilla *et al.*, 2007; Roux *et al.*, 2011). BAK1 had influence on the PTI signaling as a central regulator of PAMP-triggered immunity by integrating perception events into downstream PAMP responses as well as cell death in response to pathogen inoculation (Heese *et al.*, 2007; Dodds and Rathjen, 2010; Chaparro-Garcia *et al.*, 2011; Roux *et al.*, 2011; Schwessinger *et al.*, 2011). The

expression of *BAK1* in OERH2 was higher than that in wild-type grapes after PM-inoculation, so VpRH2 may participate in the PTI through the BAK1 pathway.

In Arabidopsis, *AtGRP7* knock-out lines show more susceptibility to *Pseudomonas syringae* infection. The *P. syringae* effector HopU1 targets RNA-binding proteins (RBPs) including AtGRP7 because of the RNA-recognition motif (RRM) and reduces the RNA-binding activity of RBPs (Fu *et al.*, 2007). AtGRP7 is ADP-ribosylated by HopU1, but R47K or R49K mutations block this modification *in vivo* and *in vitro*, so HopU1 recognizes AtGRP7 at its arginine 49 or arginine 47 (Fu *et al.*, 2007); subsequently, the recognition site of HopU1 was determined as Arg49 while Arg47 was determined as the substrate recognition (Jeong *et al.*, 2011). Interestingly, we analyzed the protein sequence of VpGRP2A and found that the positions 47 and 49 are also arginine. And so we predicted that VpGRP2A may play a similar role in biotic stress to AtGRP7.

The interaction between AtGRP7 and plant immune receptor mRNA is blocked after *Pseudomonas syringae* infection, and the level of *FLS2* and *EFR* transcripts binding to GRP7 are strongly reduced (Nicaise *et al.*, 2013). As another biotic stressor, *U. necator* may also influence the interaction between GRPs and plant immune receptor mRNA to inhibit the PTI in grapes. Free GRPs were increased after *U. necator* inoculation, and to maintain the balance of GRPs at the protein level, the transcript level of *GRP*s may decrease, as observed in our study. The transient expression assays in tobacco showed that VpGRP2A was stabilized after MG132 treatment (Fig. 7A) but there was almost no change by increasing the VpRH2 protein level (Fig. 7B), so VpGRP2A may be degraded by the 26S proteasome, but may not be degraded by VpRH2. The VpGRP2A protein level did not obviously change and maintained a relatively high level. And by qRT-PCR, we found that the transcriptional level of *VpRH2* was increased by co-expression with *VpGRP2A* (Fig. 8A, B), so the interaction between VpRH2 and VpGRP2A may be due to the RRM domain and there may be a similar model to the interaction between AtGRP7 and FLS2 or EFR (Nicaise *et al.*, 2013).

In plant immunity, NPR1 and its downstream gene *PR1* play the important roles in salicylic acid- (SA-) mediated defense response (Cao *et al.*, 1997; Feys and Parker, 2000). In this study, the expression of *PR1* and *NPR1* was more sensitive in transgenic grapes; but *PR3*, a key gene for the jasmonate- (JA-) mediated signaling pathway, showed almost no change between the transgenic and wild-type plants (Fig. 10). From this result, we predict that the RING-type ubiquitin ligase VpRH2 may influence SA-mediated, but not JA-mediated, plant immunity to enhance the resistance to PM (Feys and Parker, 2000).

In summary, the expressions of *VpRH2* and *VpGRP2A* were induced by *U. necator* inoculation, and *VpGRP2A* positively regulated the transcript level of *VpRH2* and overexpression of *VpRH2* enhanced the resistance to PM in Thompson Seedless grapes. VpRH2 interacted with VpGRP2A at the protein level and VpGRP2A was degraded by the UPS, but VpRH2 did not promote this process. On the contrary, overexpression of *VpGRP2A* enhanced the expression of *VpRH2* at the transcript level, and highly expressed *VpRH2* inhibited the expression of *VpGRP2A*. Since VpGRP2A was degraded via the UPS, so we predict that VpGRP2A may be degraded by another ubiquitin ligase, and VpRH2 may also have another interaction protein to perform its E3 activity. This hypothesis needs further research to complete the full picture for PM-resistant gene cascades.

Supplementary data

Supplementary data are available at *JXB* online.

Fig. S1. Amino acid sequence alignment of VpRH2 and VvRH2.

Fig. S2. The chromosome location and sequence of the *VpRH2* promoter.

Fig. S3. Nucleotide sequence alignment of the promoters of *VpRH2* and *VvRH2*.

Fig. S4. Molecular analysis of 12 selected OERH2 transgenic Thompson Seedless lines.

Table S1. List of primers used in this study.

Table S2. The GenBank accession numbers of the *ATL* gene family in *V. vinifera*.

Acknowledgements

This study was supported by the National Natural Science Foundation of China (grant no. 31171924). The authors thank Dr Alison H. at Wiley Editing Services for useful language editing and comments that have greatly improved the manuscript.

References

Aguilar-Hernández V, Aguilar-Henonin L, Guzmán P. 2011. Diversity in the architecture of ATLs, a family of plant ubiquitin-ligases, leads to recognition and targeting of substrates in different cellular environments. PLoS ONE **6,** e23934.

Alonso-Villaverde V, Voinesco F, Viret O, Spring JL, Gindro K. 2011. The effectiveness of stilbenes in resistant Vitaceae: ultrastructural and biochemical events during *Plasmopara viticola* infection process. Plant Physiology and Biochemistry **49,** 265–274.

Baur JA, Pearson KJ, Price NL, *et al*. 2006. Resveratrol improves health and survival of mice on a high-calorie diet. Nature **444,** 337–342.

Baur JA, Sinclair DA. 2006. Therapeutic potential of resveratrol: the *in vivo* evidence. Nature reviews. Drug Discovery **5,** 493–506.

Berrocal-Lobo M, Stone S, Yang X, Antico J, Callis J, Ramonell KM, Somerville S. 2010. ATL9, a RING zinc finger protein with E3 ubiquitin ligase activity implicated in chitin- and NADPH oxidase-mediated defense responses. PLoS ONE **5,** e14426.

Bouquet A, Torregrosa L, Iocco P, Thomas MR. 2008. Grapes. In: Kole C, Hall TC, eds. Compendium of transgenic crop plants: transgenic temperate fruits and nuts. Oxford, UK: Blackwell Publishing, 189–232.

Brewer MT, Milgroom MG. 2010. Phylogeography and population structure of the grape powdery mildew fungus, *Erysiphe necator*, from diverse *Vitis* species. BMC Evolutionary Biology **10,** 268.

Bueso E, Rodriguez L, Lorenzo-Orts L, Gonzalez-Guzman M, Sayas E, Muñoz-Bertomeu J, Ibañez C, Serrano R, Rodriguez PL. 2014. The single-subunit RING-type E3 ubiquitin ligase RSL1 targets PYL4 and PYR1 ABA receptors in plasma membrane to modulate abscisic acid signaling. The Plant Journal **80,** 1057–1071.

Cadle-Davidson L, Chicoine DR, Consolie NH. 2011. Variation within and among *Vitis* spp. for foliar resistance to the powdery mildew pathogen *Erysiphe necator*. Plant Disease **95,** 202–211.

Caffi T, Rossi V, Legler SE, Bugiani R. 2011. A mechanistic model simulating ascosporic infections by *Erysiphe necator*, the powdery mildew fungus of grapevine. Plant Pathology **60,** 522–531.

Cao H, Glazebrook J, Clarke JD, Volko S, Dong X. 1997. The Arabidopsis *NPR1* gene that controls systemic acquired resistance encodes a novel protein containing ankyrin repeats. Cell **88,** 57–63.

Chaparro-Garcia A, Wilkinson RC, Gimenez-Ibanez S, Findlay K, Coffey MD, Zipfel C, Rathjen JP, Kamoun S, Schornack S. 2011. The receptor-like kinase SERK3/BAK1 is required for basal resistance against the late blight pathogen *Phytophthora infestans* in *Nicotiana benthamiana*. PLoS ONE **6,** e16608.

Chen L, Hellmann H. 2013. Plant E3 ligases: flexible enzymes in a sessile world. Molecular Plant **6,** 1388–1404.

Chinchilla D, Zipfel C, Robatzek S, Kemmerling B, Nürnberger T, Jones JD, Felix G, Boller T. 2007. A flagellin-induced complex of the receptor FLS2 and BAK1 initiates plant defence. Nature **448,** 497–500.

Consonni C, Humphry ME, Hartmann HA, *et al*. 2006. Conserved requirement for a plant host cell protein in powdery mildew pathogenesis. Nature Genetics **38,** 716–720.

Craig A, Ewan R, Mesmar J, Gudipati V, Sadanandom A. 2009. E3 ubiquitin ligases and plant innate immunity. Journal of Experimental Botany **60,** 1123–1132.

Dai L, Zhou Q, Li R, Du Y, He J, Wang D, Cheng S, Zhang J, Wang Y. 2015. Establishment of a picloram-induced somatic embryogenesis system in *Vitis vinifera* cv. chardonnay and genetic transformation of a stilbene synthase gene from wild-growing *Vitis* species. Plant Cell, Tissue and Organ Culture **121,** 397–412.

Deb S, Sankaranarayanan S, Wewala G, Widdup E, Samuel MA. 2014. The *S*-domain receptor kinase Arabidopsis receptor Kinase2 and the U Box/Armadillo repeat-containing E3 ubiquitin ligase9 module mediates lateral root development under phosphate starvation in *Arabidopsis*. Plant Physiology **165,** 1647–1656.

Devoto A, Muskett PR, Shirasu K. 2003. Role of ubiquitination in the regulation of plant defence against pathogens. Current Opinion in Plant Biology **6,** 307–311.

Dodds PN, Rathjen JP. 2010. Plant immunity: towards an integrated view of plant–pathogen interactions. Nature Reviews. Genetics **11,** 539–548.

Dreher K, Callis J. 2007. Ubiquitin, hormones and biotic stress in plants. Annals of Botany **99,** 787–822.

Du Z, Zhou X, Li L, Su Z. 2009. plantsUPS: a database of plants' Ubiquitin Proteasome System. BMC Genomics **10,** 227.

Duplan V, Rivas S. 2014. E3 ubiquitin-ligases and their target proteins during the regulation of plant innate immunity. Frontiers in Plant Science **5,** 42.

Feechan A, Anderson C, Torregrosa L, *et al*. 2013. Genetic dissection of a TIR-NB-LRR locus from the wild North American grapevine species *Muscadinia rotundifolia* identifies paralogous genes conferring resistance to major fungal and oomycete pathogens in cultivated grapevine. The Plant Journal **76,** 661–674.

Fendrych M, Synek L, Pecenková T, Drdová EJ, Sekeres J, de Rycke R, Nowack MK, Zársky V. 2013. Visualization of the exocyst complex dynamics at the plasma membrane of *Arabidopsis thaliana*. Molecular Biology of the Cell **24,** 510–520.

Feys BJ, Parker JE. 2000. Interplay of signaling pathways in plant disease resistance. Trends in Genetics **16,** 449–455.

Fu ZQ, Guo M, Jeong BR, Tian F, Elthon TE, Cerny RL, Staiger D, Alfano JR. 2007. A type III effector ADP-ribosylates RNA-binding proteins and quells plant immunity. Nature **447,** 284–288.

Fung RW, Gonzalo M, Fekete C, Kovacs LG, He Y, Marsh E, McIntyre LM, Schachtman DP, Qiu W. 2008. Powdery mildew induces defense-oriented reprogramming of the transcriptome in a susceptible but not in a resistant grapevine. Plant Physiology **146,** 236–249.

Glawe DA. 2008. The powdery mildews: a review of the world's most familiar (yet poorly known) plant pathogens. Annual Review of Phytopathology **46,** 27–51.

González E, Solano R, Rubio V, Leyva A, Paz-Ares J. 2005. PHOSPHATE TRANSPORTER TRAFFIC FACILITATOR1 is a plant-specific SEC12-related protein that enables the endoplasmic reticulum exit of a high-affinity phosphate transporter in Arabidopsis. The Plant Cell **17,** 3500–3512.

Guzmán P. 2012. The prolific ATL family of RING-H2 ubiquitin ligases. Plant Signaling & Behavior **7,** 1014–1021.

Guzmán P. 2014. ATLs and BTLs, plant-specific and general eukaryotic structurally-related E3 ubiquitin ligases. Plant Science **215-216,** 69–75.

Hachez C, Laloux T, Reinhardt H, *et al*. 2014. Arabidopsis SNAREs SYP61 and SYP121 coordinate the trafficking of plasma membrane aquaporin PIP2;7 to modulate the cell membrane water permeability. The Plant Cell **26,** 3132–3147.

Haglund K, Dikic I. 2005. Ubiquitylation and cell signaling. The EMBO Journal **24,** 3353–3359.

Heese A, Hann DR, Gimenez-Ibanez S, Jones AM, He K, Li J, Schroeder JI, Peck SC, Rathjen JP. 2007. The receptor-like kinase SERK3/BAK1 is a central regulator of innate immunity in plants. Proceedings of the National Academy of Sciences, USA **104,** 12217–12222.

Heintzen C, Nater M, Apel K, Staiger D. 1997. AtGRP7, a nuclear RNA-binding protein as a component of a circadian-regulated negative feedback loop in *Arabidopsis thaliana*. Proceedings of the National Academy of Sciences, USA **94,** 8515–8520.

Hellmann H, Estelle M. 2002. Plant development: regulation by protein degradation. Science **297,** 793–797.

Hoefle C, Huesmann C, Schultheiss H, Börnke F, Hensel G, Kumlehn J, Hückelhoven R. 2011. A barley ROP GTPase ACTIVATING PROTEIN associates with microtubules and regulates entry of the barley powdery mildew fungus into leaf epidermal cells. The Plant Cell **23,** 2422–2439.

Hückelhoven R, Panstruga R. 2011. Cell biology of the plant–powdery mildew interaction. Current Opinion in Plant Biology **14,** 738–746.

Inada N, Higaki T, Hasezawa S. 2016. Nuclear function of subclass I actin-depolymerizing factor contributes to susceptibility in Arabidopsis to an adapted powdery mildew fungus. Plant Physiology **170,** 1420–1434.

Jang M, Cai L, Udeani GO, *et al*. 1997. Cancer chemopreventive activity of resveratrol, a natural product derived from grapes. Science **275,** 218–220.

Jefferson RA. 1987. Assaying chimeric genes in plants: the GUS gene fusion system. Plant Molecular Biology Reporter **5,** 387–405.

Jefferson RA. 1988. Plant reporter genes: the GUS gene fusion system. In: Setlow JK, ed. *Genetic engineering*, vol. **10**. Springer, 247–263.

Jeong BR, Lin Y, Joe A, *et al*. 2011. Structure function analysis of an ADP-ribosyltransferase type III effector and its RNA-binding target in plant immunity. The Journal of Biological Chemistry **286,** 43272–43281.

Jiao L, Zhang Y, Wu J, Zhang H, Lu J. 2015. A novel U-box protein gene from "Zuoshanyi" grapevine (*Vitis amurensis* Rupr. cv.) involved in cold responsive gene expression in *Arabidopsis thanliana*. Plant Molecular Biology Reporter **33,** 557–568.

Jones JD, Dangl JL. 2006. The plant immune system. Nature **444,** 323–329.

Kawasaki T, Nam J, Boyes DC, Holt BF III, Hubert DA, Wiig A, Dangl JL. 2005. A duplicated pair of Arabidopsis RING-finger E3 ligases contribute to the RPM1- and RPS2-mediated hypersensitive response. The Plant Journal **44,** 258–270.

Kim JS, Jung HJ, Lee HJ, Kim KA, Goh CH, Woo Y, Oh SH, Han YS, Kang H. 2008. Glycine-rich RNA-binding protein 7 affects abiotic stress responses by regulating stomata opening and closing in *Arabidopsis thaliana*. The Plant Journal **55,** 455–466.

Kim JS, Park SJ, Kwak KJ, Kim YO, Kim JY, Song J, Jang B, Jung CH, Kang H. 2007. Cold shock domain proteins and glycine-rich RNA-binding proteins from *Arabidopsis thaliana* can promote the cold adaptation process in *Escherichia coli*. Nucleic Acids Research **35,** 506–516.

Kim JY, Kim WY, Kwak KJ, Oh SH, Han YS, Kang H. 2010. Glycine-rich RNA-binding proteins are functionally conserved in *Arabidopsis thaliana* and *Oryza sativa* during cold adaptation process. Journal of Experimental Botany **61,** 2317–2325.

Kwak KJ, Park SJ, Han JH, Kim MK, Oh SH, Han YS, Kang H. 2011. Structural determinants crucial to the RNA chaperone activity of glycine-rich RNA-binding proteins 4 and 7 in *Arabidopsis thaliana* during the cold adaptation process. Journal of Experimental Botany **62,** 4003–4011.

Lai J, Chen H, Teng K, *et al*. 2009. RKP, a RING finger E3 ligase induced by BSCTV C4 protein, affects geminivirus infection by regulation of the plant cell cycle. The Plant Journal **57,** 905–917.

Lazaro A, Mouriz A, Piñeiro M, Jarillo JA. 2015. Red light-mediated degradation of CONSTANS by the E3 ubiquitin ligase HOS1 regulates photoperiodic flowering in Arabidopsis. The Plant Cell **27,** 2437–2454.

Lee DH, Choi HW, Hwang BK. 2011. The pepper E3 ubiquitin ligase RING1 gene, *CaRING1*, is required for cell death and the salicylic acid-dependent defense response. Plant Physiology **156,** 2011–2025.

Lescot M, Déhais P, Thijs G, Marchal K, Moreau Y, Van de Peer Y, Rouzé P, Rombauts S. 2002. PlantCARE, a database of plant *cis*-acting regulatory elements and a portal to tools for in *silico* analysis of promoter sequences. Nucleic Acids Research **30,** 325–327.

Li H, Xu Y, Xiao Y, Zhu Z, Xie X, Zhao H, Wang Y. 2010. Expression and functional analysis of two genes encoding transcription factors, *VpWRKY1* and *VpWRKY2*, isolated from Chinese wild *Vitis pseudoreticulata*. Planta **232,** 1325–1337.

Lipka U, Fuchs R, Lipka V. 2008. Arabidopsis non-host resistance to powdery mildews. Current Opinion in Plant Biology **11,** 404–411.

Liu L, Zhang Y, Tang S, Zhao Q, Zhang Z, Zhang H, Dong L, Guo H, Xie Q. 2010. An efficient system to detect protein ubiquitination by agroinfiltration in *Nicotiana benthamiana*. The Plant Journal **61,** 893–903.

Lu D, Lin W, Gao X, *et al*. 2011. Direct ubiquitination of pattern recognition receptor FLS2 attenuates plant innate immunity. Science **332,** 1439–1442.

Maekawa S, Inada N, Yasuda S, Fukao Y, Fujiwara M, Sato T, Yamaguchi J. 2014. The carbon/nitrogen regulator ARABIDOPSIS TOXICOS EN LEVADURA31 controls papilla formation in response to powdery mildew fungi penetration by interacting with SYNTAXIN OF PLANTS121 in Arabidopsis. Plant Physiology **164,** 879–887.

Mangeon A, Junqueira RM, Sachetto-Martins G. 2010. Functional diversity of the plant glycine-rich proteins superfamily. Plant Signaling & Behavior **5,** 99–104.

Marino D, Froidure S, Canonne J, Ben Khaled S, Khafif M, Pouzet C, Jauneau A, Roby D, Rivas S. 2013. *Arabidopsis* ubiquitin ligase MIEL1 mediates degradation of the transcription factor MYB30 weakening plant defence. Nature Communications **4,** 1476.

Marino D, Peeters N, Rivas S. 2012. Ubiquitination during plant immune signaling. Plant Physiology **160,** 15–27.

Martínez-García M, Garcidueñas-Piña C, Guzmán P. 1996. Gene isolation in *Arabidopsis thaliana* by conditional overexpression of cDNAs toxic to *Saccharomyces cerevisiae*: identification of a novel early response zinc-finger gene. Molecular & General Genetics **252,** 587–596.

Menzies J, Bowen P, Ehret D, Glass AD. 1992. Foliar applications of potassium silicate reduce severity of powdery mildew on cucumber, muskmelon, and zucchini squash. Journal of the American Society for Horticultural Science **117,** 902–905.

Morreale FE, Walden H. 2016. Types of ubiquitin ligases. Cell **165,** 248–248.e1.

Muthmann R. 2007. *The use of plant protection products in the European Union*. Eurostat statistical books. European Commission: Luxembourg.

Nicaise V, Joe A, Jeong BR, Korneli C, Boutrot F, Westedt I, Staiger D, Alfano JR, Zipfel C. 2013. *Pseudomonas* HopU1 modulates plant immune receptor levels by blocking the interaction of their mRNAs with GRP7. The EMBO Journal **32,** 701–712.

Opalski KS, Schultheiss H, Kogel KH, Hückelhoven R. 2005. The receptor-like MLO protein and the RAC/ROP family G-protein RACB modulate actin reorganization in barley attacked by the biotrophic powdery mildew fungus *Blumeria graminis* f.sp. *hordei*. The Plant Journal **41,** 291–303.

Pandey KB, Rizvi SI. 2009. Plant polyphenols as dietary antioxidants in human health and disease. Oxidative Medicine and Cellular Longevity **2,** 270–278.

Park CH, Chen S, Shirsekar G, *et al*. 2012. The *Magnaporthe oryzae* effector AvrPiz-t targets the RING E3 ubiquitin ligase APIP6 to suppress pathogen-associated molecular pattern-triggered immunity in rice. The Plant Cell **24,** 4748–4762.

Paumi CM, Menendez J, Arnoldo A, *et al*. 2007. Mapping protein–protein interactions for the yeast ABC transporter Ycf1p by integrated split-ubiquitin membrane yeast two-hybrid analysis. Molecular Cell **26,** 15–25.

Phan HA, Iacuone S, Li SF, Parish RW. 2011. The MYB80 transcription factor is required for pollen development and the regulation of tapetal programmed cell death in *Arabidopsis thaliana*. The Plant Cell **23,** 2209–2224.

Roux M, Schwessinger B, Albrecht C, *et al*. 2011. The *Arabidopsis* leucine-rich repeat receptor-like kinases BAK1/SERK3 and BKK1/SERK4 are required for innate immunity to hemibiotrophic and biotrophic pathogens. The Plant Cell **23,** 2440–2455.

Santos-Rosa M, Poutaraud A, Merdinoglu D, Mestre P. 2008. Development of a transient expression system in grapevine via agro-infiltration. Plant Cell Reports **27,** 1053–1063.

Schöning JC, Streitner C, Page DR, Hennig S, Uchida K, Wolf E, Furuya M, Staiger D. 2007. Auto-regulation of the circadian slave oscillator component AtGRP7 and regulation of its targets is impaired by a single RNA recognition motif point mutation. The Plant Journal **52,** 1119–1130.

Schwessinger B, Roux M, Kadota Y, Ntoukakis V, Sklenar J, Jones A, Zipfel C. 2011. Phosphorylation-dependent differential regulation of plant growth, cell death, and innate immunity by the regulatory receptor-like kinase BAK1. PLoS Genetics **7,** e1002046.

Schwessinger B, Zipfel C. 2008. News from the frontline: recent insights into PAMP-triggered immunity in plants. Current Opinion in Plant Biology **11,** 389–395.

Serrano I, Gu Y, Qi D, Dubiella U, Innes RW. 2014. The *Arabidopsis* EDR1 protein kinase negatively regulates the ATL1 E3 ubiquitin ligase to suppress cell death. The Plant Cell **26,** 4532–4546.

Serrano M, Parra S, Alcaraz LD, Guzmán P. 2006. The ATL gene family from *Arabidopsis thaliana* and *Oryza sativa* comprises a large number of putative ubiquitin ligases of the RING-H2 type. Journal of Molecular Evolution **62,** 434–445.

Smoliga JM, Baur JA, Hausenblas HA. 2011. Resveratrol and health – A comprehensive review of human clinical trials. Molecular Nutrition & Food Research **55,** 1129–1141.

Stegmann M, Anderson RG, Ichimura K, Pecenkova T, Reuter P, Žárský V, McDowell JM, Shirasu K, Trujillo M. 2012. The ubiquitin ligase PUB22 targets a subunit of the exocyst complex required for PAMP-triggered responses in Arabidopsis. The Plant Cell **24,** 4703–4716.

Stone SL, Hauksdóttir H, Troy A, Herschleb J, Kraft E, Callis J. 2005. Functional analysis of the RING-type ubiquitin ligase family of Arabidopsis. Plant Physiology **137,** 13–30.

Szkudelski T, Szkudelska K. 2015. Resveratrol and diabetes: from animal to human studies. Biochimica et Biophysica Acta **1852,** 1145–1154.

Tak H, Mhatre M. 2013. Molecular characterization of *VvSDIR1* from *Vitis vinifera* and its functional analysis by heterologous expression in *Nicotiana tabacum*. Protoplasma **250,** 565–576.

Tan Y, Qin Y, Li Y, Li M, Ma F. 2014. Overexpression of MpGR-RBP1, a glycine-rich RNA-binding protein gene from *Malus prunifolia* (Willd.) Borkh., confers salt stress tolerance and protects against oxidative stress in *Arabidopsis*. Plant Cell, Tissue and Organ Culture **119,** 635–646.

Trouvelot S, Varnier AL, Allègre M, *et al*. 2008. A beta-1,3 glucan sulfate induces resistance in grapevine against *Plasmopara viticola* through priming of defense responses, including HR-like cell death. Molecular Plant-Microbe Interactions **21,** 232–243.

Trujillo M, Ichimura K, Casais C, Shirasu K. 2008. Negative regulation of PAMP-triggered immunity by an E3 ubiquitin ligase triplet in Arabidopsis. Current Biology **18,** 1396–1401.

Trujillo M, Shirasu K. 2010. Ubiquitination in plant immunity. Current Opinion in Plant Biology **13,** 402–408.

Vierstra RD. 2009. The ubiquitin-26S proteasome system at the nexus of plant biology. Nature Reviews. Molecular Cell Biology **10,** 385–397.

Waadt R, Schmidt LK, Lohse M, Hashimoto K, Bock R, Kudla J. 2008. Multicolor bimolecular fluorescence complementation reveals simultaneous formation of alternative CBL/CIPK complexes in *planta*. The Plant Journal **56,** 505–516.

Wang S, Liang D, Shi S, Ma F, Shu H, Wang R. 2010. Isolation and characterization of a novel drought responsive gene encoding a glycine-rich RNA-binding Protein in *Malus prunifolia* (Willd.) Borkh. Plant Molecular Biology Reporter **29,** 125–134.

Wang W, Devoto A, Turner JG, Xiao S. 2007. Expression of the membrane-associated resistance protein RPW8 enhances basal defense against biotrophic pathogens. Molecular Plant-Microbe Interactions **20,** 966–976.

Wang W, Vignani R, Scali M, Cresti M. 2006. A universal and rapid protocol for protein extraction from recalcitrant plant tissues for proteomic analysis. Electrophoresis **27,** 2782–2786.

Wang Y, Liu Y, He P, Chen J, Lamikanra O, Lu J. 1995. Evaluation of foliar resistance to *Uncinula necator* in Chinese wild *Vitis* Species. Vitis **34,** 159–164.

Xiao S, Ellwood S, Calis O, Patrick E, Li T, Coleman M, Turner JG. 2001. Broad-spectrum mildew resistance in *Arabidopsis thaliana* mediated by RPW8. Science **291,** 118–120.

Xu W, Yu Y, Ding J, Hua Z, Wang Y. 2010. Characterization of a novel stilbene synthase promoter involved in pathogen- and stress-inducible expression from Chinese wild *Vitis pseudoreticulata*. Planta **231,** 475–487.

Xu W, Yu Y, Zhou Q, Ding J, Dai L, Xie X, Xu Y, Zhang C, Wang Y. 2011. Expression pattern, genomic structure, and promoter analysis of the gene encoding stilbene synthase from Chinese wild *Vitis pseudoreticulata*. Journal of Experimental Botany **62,** 2745–2761.

Yoo SD, Cho YH, Sheen J. 2007. *Arabidopsis* mesophyll protoplasts: a versatile cell system for transient gene expression analysis. Nature Protocols **2,** 1565–1572.

Yu Y, Xu W, Wang J, Wang L, Yao W, Xu Y, Ding J, Wang Y. 2013*a*. A core functional region of the RFP1 promoter from Chinese wild grapevine is activated by powdery mildew pathogen and heat stress. Planta **237,** 293–303.

Yu Y, Xu W, Wang J, *et al*. 2013*b*. The Chinese wild grapevine (*Vitis pseudoreticulata*) E3 ubiquitin ligase *Erysiphe necator*-induced RING finger protein 1 (EIRP1) activates plant defense responses by inducing proteolysis of the VpWRKY11 transcription factor. The New Phytologist **200,** 834–846.

Yu Y, Xu W, Wang S, Xu Y, Li H, Wang Y, Li S. 2011. *VpRFP1*, a novel C4C4-type RING finger protein gene from Chinese wild *Vitis pseudoreticulata*, functions as a transcriptional activator in defence response of grapevine. Journal of Experimental Botany **62,** 5671–5682.

Zabka V, Stangl M, Bringmann G, Vogg G, Riederer M, Hildebrandt U. 2008. Host surface properties affect prepenetration processes in the barley powdery mildew fungus. The New Phytologist **177,** 251–263.

Zhang B, Karnik R, Wang Y, Wallmeroth N, Blatt MR, Grefen C. 2015. The Arabidopsis R-SNARE VAMP721 interacts with KAT1 and KC1 K^+ channels to moderate K^+ current at the plasma membrane. The Plant Cell **27,** 1697–1717.

Zhou Q, Dai L, Cheng S, He J, Wang D, Zhang J, Wang Y. 2014. A circulatory system useful both for long-term somatic embryogenesis and genetic transformation in *Vitis vinifera* L. cv. Thompson Seedless. Plant Cell, Tissue and Organ Culture **118,** 157–168.

Zhu Y, Li Y, Fei F, *et al*. 2015. E3 ubiquitin ligase gene *CMPG1-V* from *Haynaldia villosa* L. contributes to powdery mildew resistance in common wheat (*Triticum aestivum* L.). The Plant Journal **84,** 154–168.

Zhu Z, Shi J, Cao J, He M, Wang Y. 2012*a*. *VpWRKY3*, a biotic and abiotic stress-related transcription factor from the Chinese wild *Vitis pseudoreticulata*. Plant Cell Reports **31,** 2109–2120.

Zhu Z, Shi J, He M, Cao J, Wang Y. 2012*b*. Isolation and functional characterization of a transcription factor *VpNAC1* from Chinese wild *Vitis pseudoreticulata*. Biotechnology Letters **34,** 1335–1342.

Zhu Z, Shi J, Xu W, *et al*. 2013. Three ERF transcription factors from Chinese wild grapevine *Vitis pseudoreticulata* participate in different biotic and abiotic stress-responsive pathways. Journal of Plant Physiology **170,** 923–933.